Journal of Iberian Geology
https://doi.org/10.1007/s41513-024-00254-w

RESEARCH PAPER

Environmental conditions in the pre-Jenkyns event times (late Pliensbachian—early Toarcian) in the South Iberian Palaeomargin (Betic External Zones, Southern Spain)

L. M. Nieto[1] · C. Ayadi[1] · Á. Fraguas[2] · J. M. Molina[1] · M. Reolid[1]

Received: 29 March 2024 / Accepted: 24 July 2024

Abstract

Three stratigraphic sections of the Betic External Zones were studied, two from the Median Subbetic (PEL and PR) and one from the External Subbetic (CE). The upper Pliensbachian materials and the transition to the lower Toarcian were dated with calcareous nannofossils in PEL and PR in this paper, while in the CE section, previous ammonite and nannofossil biostratigraphies were considered. The dominant facies are alternance of marly limestone—marl, although in the CE section, the Toarcian is represented by marls, where the Jenkyns Event has been recorded. In terms of ichnofossils, in the PEL section *Macaronichnus* predominates. In the PR and CE sections, the ichnoassemblages are dominated by *Planolites*, *Thalassinoides* and *Chondrites*. The facies and ichnofacies distinguished formed in pelagic or hemipelagic marine environments. Analysis of the correlation between $\delta^{13}C$ and $\delta^{18}O$ and of each of them with Sr and Fe/Ca and Sr/Ca, as well as the Z-factor, indicate that the geochemical signal has not been modified by diagenesis. In the PEL and PR sections, the $\delta^{13}C$ and $\delta^{18}O$ ratios do not allow to clearly identify isotopic events, except in CE where the Jenkyns Event was recorded. The proxies used to study detritism (Zr/Rb, Sr/Cu, Chemical Index Alteration, CIA, and C-value) show trends opposite to those detected in other Tethys sections and even between them. These peculiarities in the geochemical data are interpreted as the result of the opening of the Hispanic Corridor, the mixing of Panthalassa and Tethys seawaters and extensional tectonics, which favoured the development of half grabens with significant differential subsidence, especially during the NJT5b Subzone (latest Pliensbachian). These half grabens could be affected by contourite currents according to the *Macaronichnus* assemblage in some of these sections.

Keywords Early Jurassic · Southern Iberian Palaeomargin · Ichnofossils · Calcareous nannofossil biostratigraphy · Geochemical proxies of detritism · Hispanic Corridor · Contourite currents

Resumen

Se estudiaron tres secciones estratigráficas de las Zonas Externas Béticas, dos del Subbético Medio (PEL y PR) y una del Subbético Externo (CE). En PEL y PR se dataron con nanofósiles calcáreos los materiales del Pliensbachiense superior y la transición al Toarciense inferior, mientras que en la sección CE se consideraron bioestratigrafías previas de ammonites y nanofósiles. Las facies dominantes son alternancias de calizas margosas—margas, aunque en la sección CE, el Toarciense

✉ L. M. Nieto
lmnieto@ujaen.es

C. Ayadi
ca000025@red.ujaen.es

Á. Fraguas
angela.fraguas@urjc.es

J. M. Molina
jmmolina@ujaen.es

M. Reolid
mreolid@ujaen.es

[1] Departamento de Geología y Centro de Estudios Avanzados en Ciencias de la Tierra, Energía y Medio Ambiente (CEACTEMA), Universidad de Jaén. Campus Universitario Las Lagunillas, 23071 Jaén, Spain

[2] Departamento de Biología, Geología, Física y Química Inorgánica y Grupo de Investigación en Dinámica de la Tierra y Evolución del Paisaje (DYNAMICAL), Universidad Rey Juan Carlos, 28933 Móstoles, Spain

Published online: 18 October 2024

está representado por margas, donde se ha registrado el Evento Jenkyns. En cuanto a los icnofósiles, en la sección PEL predomina *Macaronichnus*. En las secciones PR y CE, las icnoasociaciones están dominadas por *Planolites*, *Thalassinoides* y *Chondrites*. Se distinguen facies e icnofacies formadas en ambientes marinos pelágicos o hemipelágicos. El análisis de la correlación entre $\delta^{13}C$ y $\delta^{18}O$ y de cada uno de ellos con Sr y Fe/Ca y Sr/Ca, así como el factor Z, indican que la señal geoquímica no ha sido modificada por diagénesis. En las secciones PEL y PR, las relaciones $\delta^{13}C$ y $\delta^{18}O$ no permiten identificar claramente eventos isotópicos, excepto en CE donde se registró el Evento Jenkyns. Los proxies utilizados para estudiar el detritismo (Zr/Rb, Sr/Cu, Índice de Alteración Química, CIA, y valor-C) muestran tendencias opuestas a las detectadas en otras secciones del Tethys e incluso entre ellas. Estas peculiaridades en los datos geoquímicos se interpretan como el resultado de la apertura del Corredor Hispánico, la mezcla de aguas marinas de Panthalassa y Tethys y la tectónica extensional, que favoreció el desarrollo de semigrabens con importante subsidencia diferencial, especialmente durante la Subzona NJT5b (Pliensbachiense terminal). Estos semigrabens podrían estar afectados por corrientes de contorno a tenor de la presencia de *Macaronichnus* en algunas de estas secciones.

Palabras clave Jurásico Inferior · Paleomargen Suribérico · Icnofósiles · Bioestratigrafía de nanofósiles calcáreos · Proxies geoquímicos de detritismo · Corredor Hispánico · Corrientes de contorno

1 Introduction

The Pliensbachian was a very dynamic Jurassic stage, in which very important changes took place: (1) palaeogeographic (opening of the Hispanic Corridor; Dera et al., 2009a, 2009b; Krencker et al., 2019; and references herein), (2) palaeoclimatic (waxing and waning of ice caps as a consequence of declines and rises in seawater temperature; Bougeault et al., 2017; Gómez et al., 2016; Krencker et al., 2019; Price et al., 2016; and references herein), and (3) palaeoceanographic (modification of the marine current system in the Tethys, Boreal and Central Atlantic; Bodin et al., 2016, 2023; Dera et al., 2009a, for example). All these events induced shifts of different orders in global seawater chemistry (Price et al., 2016). While long-lived events have been associated with variations in CO_2 concentration, short-term changes are difficult to explain (e.g., Price et al., 2016).

Based on isotopic data, the early Pliensbachian has been interpreted as a warming interval (ranging from 16 ºC to 18 ºC in the Asturian Basin of North Iberia according to Gómez et al., 2016). This climatic trend covered the Ibex and Davoei zones and the earliest part of the Lavinianum Zone. A subsequent cooling occurred during the late Pliensbachian that may have promoted the formation of high-latitudinal glaciation at their most extensive in the latest Pliensbachian to earliest Toarcian (Dera et al., 2011; Gómez et al., 2016; Korte & Hesselbo, 2011; Ruebsam & Schwark, 2021; Ruebsam et al., 2019). Latest Pliensbachian to early Toarcian equatorial sea surface temperatures fluctuated between 22 ºC and 32 °C, attesting to highly variable and contrasting climate conditions (Ruebsam et al., 2020a). During the early Toarcian, related to the Jenkyns Event carbon cycle perturbation, seawater temperature in the tropical to subtropical latitudes raised by about 10 °C (Ruebsam et al., 2020a). Sea-level changes were related to these climatic changes. Therefore, the end Pliensbachian is characterized by a sea-level fall with subsequent flooding and a negative Carbon Isotope Excursion (CIE) related to the Pliensbachian-Toarcian boundary event (Bodin et al., 2016; Fantasia et al., 2019; Fleischmann et al., 2022; Rodrigues et al., 2019).

Bougeault et al. (2017), based on the study of the kaolinite/illite ratio, recognized a decrease in the runoff occurred at the end of Pliensbachian stage, considering that a cold stage, possibly associated with cold ice cap growth, has also been recorded in this time interval (Bodin et al., 2023; Bougeault et al., 2017; Gómez et al., 2016; Krencker et al., 2019; among others). However, Bougeault et al. (2017) also recognized minor oscillations in kaolinite/illite ratio values during the late Pliensbachian interpreted as oscillations in runoff.

A factor to consider in the development of the climate changes during the Pliensbachian is the modification of the oceanic current system due to palaeogeographic changes (tectonically driven) and sea-level variations (Dera et al., 2009a, 2009b; Price et al., 2016). Prior to the opening of the Hispanic Corridor (Davoei-Lavinianum zones; early-late Pliensbachian transition), isotopic data support the idea of a flow from the Boreal domains into the Tethyan Ocean via the Viking Corridor (Dera et al., 2009a). The opening of the Hispanic Corridor led to a change in the oceanic circulation system, such that a current develops through this palaeogeographic feature connecting Panthalassa with the Tethys. On the other hand, the formation of this corridor also favoured the establishment of a current from the Tethys and Panthalassa Oceans towards the Boreal Domain (e.g., Dera et al., 2009a, 2009b).

The opening of the Hispanic Corridor was associated with the rifting process and the beginning of the formation of the Central Atlantic. This developed a major system of tilted blocks and small, generally, shallow sub-basins. In addition, in connection with the rifting, an increase in volcanic activity related to the Central Atlantic Magmatic Province and the Karoo-Ferrar Large Igneous Province (LIP) took place

(Franceschi et al., 2014; Krencker et al., 2022; Schöllhorn et al., 2020a, 2020b; among others).

During the Pliensbachian, the South Iberian Palaeomargin (SIP), was affected by these tectonic, palaeoclimatic and palaeoceanographic processes according to its palaeogeographic position (Vera, 2004; Ruiz-Ortiz et al., 2019; Nieto et al., 2023; among others). As a consequence of rifting and the opening of the Hispanic Corridor, the shallow carbonate platform developed during the Hettangian and Sinemurian (represented by the Gavilán Formation) collapsed. Numerous tilted blocks were formed, bringing about the sedimentary record very changeable both in sedimentation rate and facies, with blocks in which wide hiatuses developed and others with more continuous sedimentary record (Nieto et al., 2023). The sediments deposited were marly limestones and marls with a clear hemipelagic and pelagic nature (represented by the Zegrí Formation). During the late Pliensbachian, alternating marly limestones and marl predominate, whereas, coinciding with the beginning of the Toarcian, mainly marly sedimentation deposited. In addition, the chemistry of the SIP waters must have undergone changes due to modifications in the oceanic circulation system. The progressive opening of the Hispanic Corridor (early-late Pliensbachian transition), favoured the developing of a current pattern affecting the SIP from Panthalassa and from Tethys towards Boreal domains (e.g., Dera et al., 2009a; Nieto et al., 2023; Price et al., 2016). The chemistry of the seawaters would also be influenced by the contributions of continental waters, which would reflect the weathering processes from the Iberian massif.

The record of the oxygen depleted conditions (Toarcian Oceanic Anoxic Event or T-OAE) related to the Jenkyns Event is very irregular in the SIP, being confined to small, more subsiding pelagic basins where locally suboxic facies developed (e.g. Reolid et al., 2014, 2021). As in other areas of the Tethys where the T-OAE is recorded, this event and the environmental conditions that prevailed during its development are well known in the SIP (e.g. Rodríguez-Tovar & Uchman, 2010; Rodríguez-Tovar & Reolid, 2013; Reolid et al., 2014, 2015; Rodrigues et al., 2019; Ruebsam et al., 2020b; Kovacs et al., 2024). However, the environmental changes that preceded the development of this event need to be further investigated, as it is also for the SIP. The aim of this paper is to analyze the environmental conditions at this palaeomargin in the time just before the Jenkyns Event (late Pliensbachian-earliest Toarcian). The influence of water runoff on sedimentation occurring in the SIP, mainly during the late Pliensbachian and the Pliensbachian-Toarcian transition, will be discussed. This will bring us some light about the prevailing climatic conditions that conditioned continental weathering. For this purpose, a multi-proxy analysis of different detrital ratios, such as Zr/Rb, Sr/Cu, Chemical Index Alteration (CIA) and C-value, will be carried out on samples taken from three stratigraphic sections from the Subbetic (Betic Cordillera) with Pliensbachian and lower Toarcian records.

2 Geological setting

The studied sections belong to the Lower Jurassic of the Subbetic, in the External Zones of the Betic Cordillera (SE Spain), which is the westernmost Alpine Mediterranean Chain, being 600 km long and 200 km wide (García-Hernández et al., 1980). The Betic Cordillera is subdivided into the Internal and the External Zones. The External Zones represent the SIP that developed during the Mesozoic in the westernmost Tethys, approximately at 20º N during the Early Jurassic (Bassoullet et al., 1993), and can be further divided into Prebetic (more proximal areas) and Subbetic (more distal areas) domains (Fig. 1). The Subbetic is subdivided from north to south in Intermediate Domain, External, Median, and Internal. The studied sections are located in the External and Median Subbetic (Fig. 1). The Lower Jurassic of the Subbetic is composed by the Gavilán and Zegrí formations. The Gavilán Formation (Hettangian-lower Pliensbachian) represents platform carbonates (crinoidal limestones, oolitic and oncolitic limestones, cherty limestones and dolostones) and the Zegrí Formation (upper Pliensbachian-lower Bajocian) is composed of pelagic and hemipelagic deposits (marly limestones and marls and marly Ammonitico Rosso). Both formations are limited at the base by the intra-Pliensbachian discontinuity. The thickness of the Zegrí Formation ranges from just a few metres to 500 m in the External and Median Subbetic (Nieto et al., 2004). The lower part of the Zegrí Formation (Pliensbachian-lower Toarcian) is made up of marly limestone-marl rhythmites and marls. The middle-upper Toarcian is commonly represented by cherty limestones and red nodular marly limestones (marly Ammonitico Rosso facies) (Molina, 1987; Reolid et al., 2015).

Three stratigraphic sections have been considered: Sierra Pelada (PEL), Puente Romano (PR) and La Cerradura (CE) (Figs. 1, 2). The PEL and PR sections are located in the Median Subbetic and were previously studied by González-Donoso et al. (1971) and Jiménez (1986) with regard to ammonite biostratigraphy. The CE section was attributed to the External Subbetic; the ammonites present in this section, were initially studied by Braga (1983) and Jiménez (1986). Later, the CE section was investigated, from an ichnological and geochemical point of view, by Reolid et al. (2014) and Silva et al. (2021) among others.

The Sierra Pelada (PEL) section is located to the north of Sierra Pelada ravine, 200 m NE of the Cortijo del Madroñal, province of Granada (section bottom coordinates: 37º20′24.3″ N; 3º53′44.6″ W). The Puente Romano (PR) section is located near the roman bridge on the Colomera

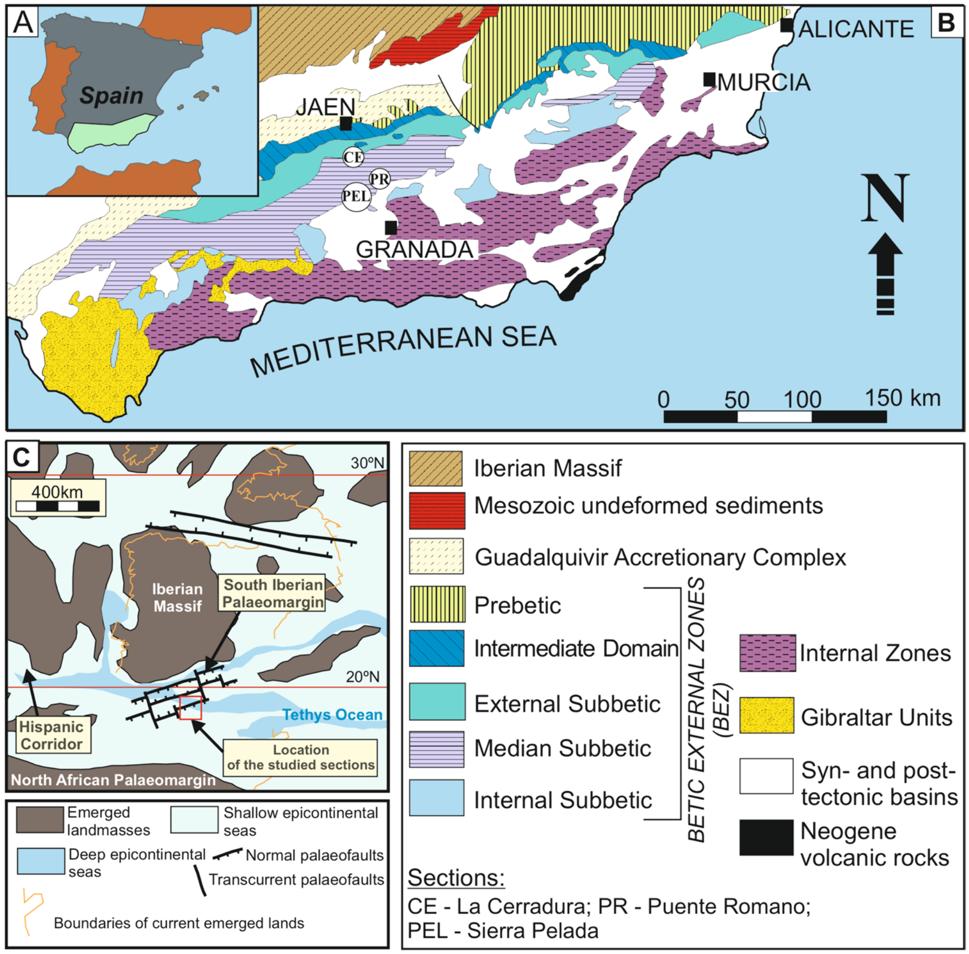

Fig. 1 Geographical and geological setting. **A** Location of the Betic Cordillera in the South of Spain. **B** Geological sketch of the Betic Cordillera with location of the stratigraphic sections studied (CE: La Cerradura; PR: Puente Romano; PEL: Sierra Pelada). **C** Palaeogeographic sketch of the Pliensbachian with the location of the South Iberian Palaeomargin and the Hispanic Corridor (modified from Nieto et al., 2023)

river, 500 m to the NE of the Colomera village, province of Granada (section bottom coordinates: 37º22′36.6″ N; 3º42′31.4″ W). La Cerradura (CE) section is in the E trench of motorway A-44, km 56.8, 15 km S of Jaén city (section bottom coordinates: 37º41′51.9″ N; 3º38′0.1″ W).

In the PEL and PR sections outcrops well the upper part of the Gavilán Formation, dated as lower Pliensbachian (Nieto et al., 2023 and references in this paper) and its contact with the Zegrí Formation, where the upper Pliensbachian and lower Toarcian are recorded. In the CE section upper Pliensbachian – lower Toarcian record, including the materials in which the T-OAE, was detected (Reolid et al., 2014; Ruebsam et al., 2020a, 2020b).

3 Materials and methodology

3.1 Fieldwork and facies analysis

The fieldwork in the studied sections was focused on the analyses of sedimentary structures, trace fossils, recovery of fossil macroinvertebrates and sampling for subsequent analyses of microfacies, geochemistry and calcareous nannoplankton.

We have used for the CE section the same 34 samples studied by Reolid et al. (2014). Both the PEL and PR sections were sampled on a bed by bed; 72 samples from PEL section and 49 samples from PR section. Samples from indurated marly limestones and limestones were selected for preparation of thin sections and polished slabs. Samples consisting of soft marls were selected for analyses of stable isotopes (C and O) and elemental inorganic geochemistry. For the microfacies studies, a Leica M205C binocular microscope was used to study a total of 121 thin sections. Analysis of trace fossils in the field was completed with the preparation of 22 polished slabs. The ichnological analysis included the bioturbation index (from 1 to 5, Taylor & Goldring, 1993) for quantifying the degree of bioturbation, and integrates sedimentology and ichnology. Therefore, a progressively higher degree of bioturbation results from an increased burrow overlaps and the subsequent loss of the primary sedimentary fabric.

The reference ammonite biostratigraphy used to date the materials of the studied sections follows Braga (1983)

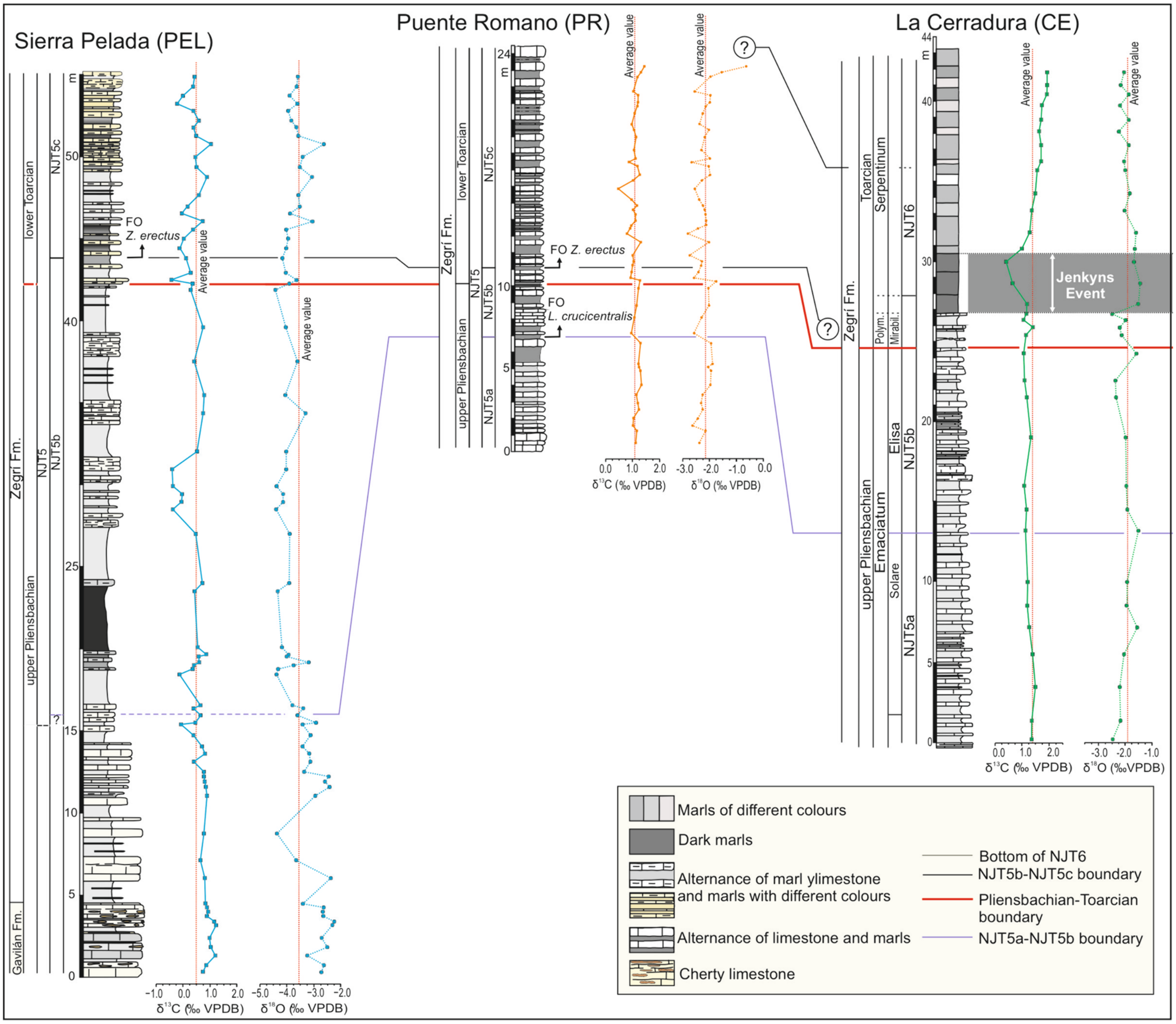

Fig. 2 Correlation of the stratigraphic sections considered in this paper. For each section the $\delta^{13}C$ (V-PDB in ‰) and $\delta^{18}O$ (V-PDB in ‰) curves with indication of the average value are represented

and Jiménez (1986) for the SIP, while for calcareous nannoplankton follows Ferreira et al. (2019) (Fig. 3). The study of calcareous nannoplankton was carried out in PEL and PR sections. The biostratigraphic framework of the CE section is based on ammonite record (Braga, 1983; Jiménez, 1986; Reolid et al., 2014), and on the calcareous nannoplankton (Reolid et al., 2014), according to the biostratigraphy of calcareous nannoplankton from Mattioli and Erba (1999).

3.2 Calcareous nannofossils

A total of 23 and 21 smear slides were prepared from the original samples collected from the PEL and the PR sections, respectively. In both cases, the standard preparation technique of Bown and Young (1998) was used, and semi-quantitative analyses were carried out with a Leica DMLP light microscope and a Leica DFC 420 digital camera at 1250 × magnification. For the PEL samples, four transverses were analyzed per sample, resulting in more than 500 fields of view, to identify rare or very rare species. Total abundance and degree of preservation of calcareous nannofossil assemblages, and the relative abundances of each species identified were obtained for each sample (see Table 1 for further details), following the approach of Perilli et al. (2010) and Fraguas et al., (2015, 2018). *Mitrolithus* spp. and *Crepidolithus* spp. include all the specimens belonging to both genera recognized in lateral view or

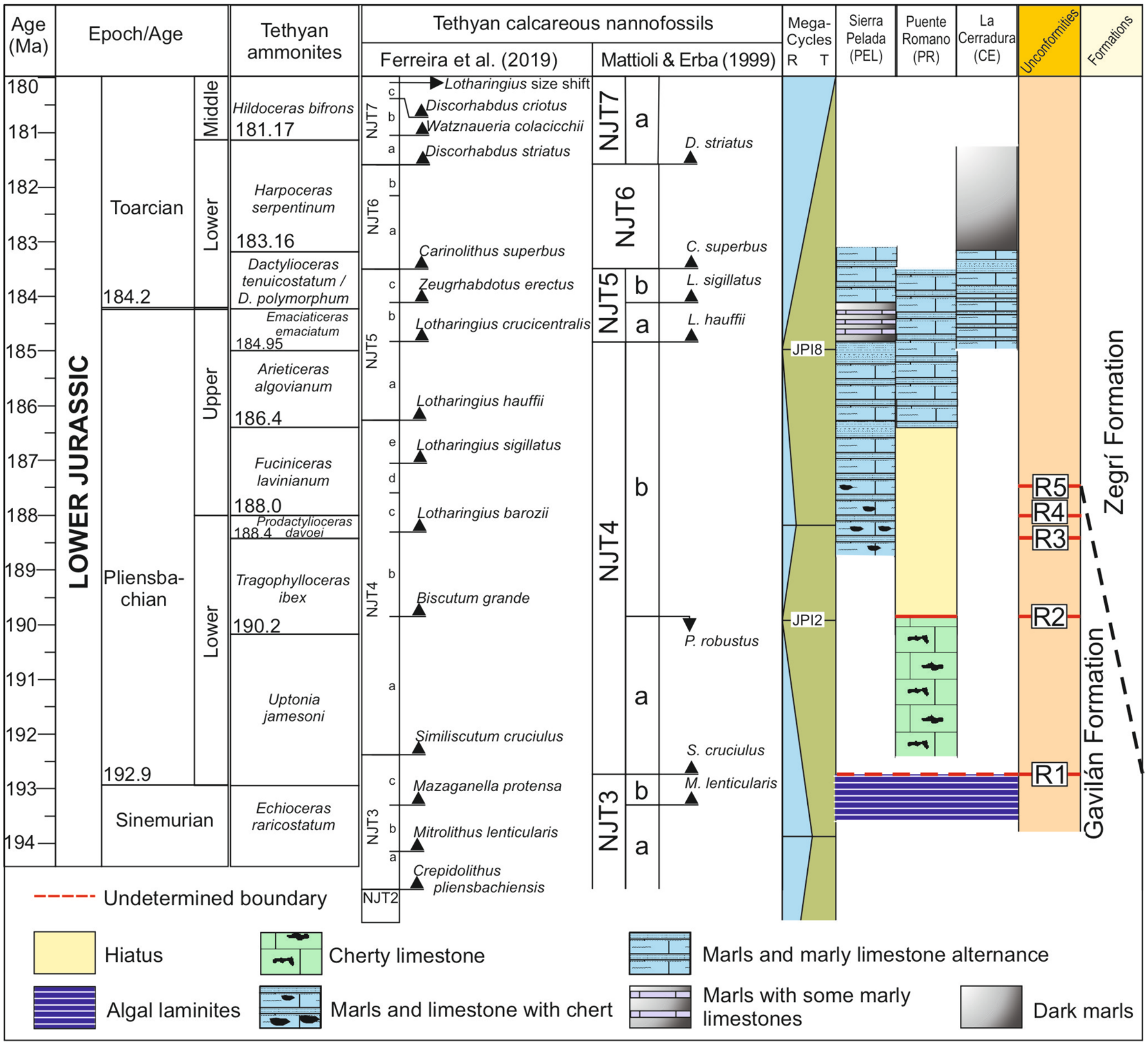

Fig. 3 Bio- and chrono- stratigraphic diagram for the Lower Jurassic (Pliensbachian-lower Toarcian) from the data obtained in the stratigraphic sections considered in this paper. The numerical ages and the Tethyan Ammonites zones are from Hesselbo et al. (2020a). The Tethyan calcareous nannofossils are from Ferreira et al. (2019) and Mattioli and Erba (1999). The unconformities R1 to R5 are from Nieto et al. (2023)

those that cannot be identified taxonomically at species level, since the diagnostic characters were not preserved. The appendix A includes all the calcareous nannofossil species mentioned within the text in alphabetical order.

From the 21 smear slides prepared from the samples taken in PR section, a total of 2000 fields of view were analyzed per sample for semiquantitative analysis, in order to identify those species very rare. The results obtained have been included in Nieto et al. (2023).

3.3 Elemental and C-O isotope geochemistry

The elemental analysis of the samples of the three sections considered in this paper were obtained in the Centro de Instrumentación Científica (CIC) of the Universidad de Granada. Whole-rock analyses of major elements were made using X-ray Fluorescence (XRF) in a Philips PW1040/10 spectrometer. Trace elements were analysed using an inductively coupled plasma-mass spectrometer (ICP-MS), the Perkin Elmer Sciex-Elan 5000.

The C and O isotopes were analyzed from bulk samples from CE section by Reolid et al. (2014), PR section by Nieto et al. (2023) and PEL section in this paper. The 72 samples of the last section were analyzed at the Laboratory of the Scientific and Technological Centre (CCiT) of the Universidad de Barcelona with a Finningan MAT 253 isotope ratio mass spectrometer with a Kiel IV carbonate analysis device (ThermoFisher Scientific). The isotope ratios obtained were referred to the VPDB standard notation in ‰. Analytical precision was kept between 0.01 and 0.05 for $\delta^{13}C$ and $\delta^{18}O$.

Table 1 Distribution chart of the calcareous nannofossils identified at Sierra Pelada (PEL) section, with the results obtained from the semiquantitative analyses. Calcareous nannofossil zones and subzones identified in this work are indicated. Main events are written in bold

Sample	N species	Abundance	Preservation	*Schizosphaerella punctulata*	*C. jansae*	*P. liasicus distinctus*	*C. crassus*	*P. liasicus liasicus*	*Crepidolithus* spp.	*C. primulus*	*C. cantabriensis*	*T. patulus*	*C. cavus*	*M. lenticularis*	*Mitrolithus* spp.	*C. granulatus*	*C. crucifer*	*Calyculus* spp.	*B. prinsii*	*B. novum*	*B. finchii*	*B. grande*	*L. hauffii*	*L. barozii*	*B. intermedium*	*L. sigilatus*	*L. crucicentralis*	*B. leufensis*	*A. atavus*	*S. arctus*	*Z. erectus*	Nannofossil Zone	Nannofossil subzone
PEL-1	12	C	M	C	F		VR					VR		R		VR	VR			VR		VR	R	VR		VR						**NJT5**	**NJT5c**
PEL-4	11	RF	M	F	VR			VR				VR		R					VR	VR	VR		R	VR		VR							
PEL-7	13	RF	M	F	R		VR	VR		VR		VR					VR					VR	VR	VR	VR	VR	VR						
PEL-10	15	F	M	F	R	VR	VR			VR		VR		VR			VR		VR		VR		VR	VR		VR	VR				VR		
PEL-13	6	VR	BM	VR	VR				VR													VR	VR	VR									
PEL-15	16	F	M	F	F		VR	VR			VR	VR	VR	R			VR		VR		VR		R	VR	VR	VR	VR						
PEL-17	16	F	M	F	F		VR	VR				VR		R			VR	VR	VR		VR	VR	VR	VR	VR	VR				VR			
PEL-20	11	F	M	F	F							VR		R			VR		VR				VR	VR		VR	VR				VR		
PEL-24 m	11	RF	BM	F	R		VR					VR		VR			VR		VR				VR	VR	VR	VR							**NJT5b**
PEL-27	2	VR	B	VR										VR																			
PEL-29	15	F	M	F	R		VR				VR	VR	VR	R	VR		VR					VR	VR	VR	VR	VR	VR						
PEL-33	13	RF	BM	F	VR		VR		VR					VR	VR		VR						VR	VR		VR	VR	VR	VR				
PEL-40 m	12	R	M	VR	R			VR				VR		VR	VR							VR	VR	VR	VR	VR	VR						
PEL-42	1	VR	B	VR																													
PEL-44 m	13	F	M	R	F	VR	VR	VR						VR	VR		VR					VR	VR	VR		VR	VR						
PEL-45	10	RF	M	R	F		VR						VR	VR	VR		VR						VR	VR			VR						
PEL-46 m	4	VR	BM	VR	VR			VR															VR										?
PEL-48t	2	VR	BM	VR	VR																											?	
PEL-52t	BARREN																																
PEL-55	2	VR	B	VR	VR																												
PEL-60	BARREN																																
PEL-62t	1	VR	B		VR																												
PEL-66	BARREN																																

Assemblage abundance classes: A = abundant (10–15 specimens in each field of view), C = common (1–10 specimens in each field of view), F = few (1 specimen in 1–10 field/s of view), R = rare (1 specimen in 11–100 fields of view), VR = very rare (1 specimen in more than 101 fields of view)

Species abundance classes: A = abundant (1–5 specimens in each field of view), C = common (1 specimen in 2–10 fields of view), F = few (1 specimen in 10–30 fields of view), R = rare (1 specimen in 31–100 fields of view), VR = very rare (1 specimen in more than 101 fields of view)

Preservation classes: G = good (the majority of the specimens show their diagnostic characteristics and only some of them are slightly etched and/or overgrown), M = moderate (the majority of the specimens are recognizable, even if some of them are etched and/or overgrown and/or fragmented), B = poor (the majority of the specimens are heavily etched or/and overgrown and/or fragmented and the identification of the species is sometimes difficult), VB = very poor (only a few specimens are recognizable)

The Chemical Index Alteration (CIA) corrected for carbonate contents, was calculated according to the expression (1) from Nesbitt and Young (1982, 1989):

$$CIA = 100 \times \frac{Al_2O_3}{Al_2O_3 + CaO + Na_2O + K_2O} \quad (1)$$

To analyze the influence of diagenesis in the primary geochemistry signal, the Z factor was used, calculated for each studied section according to the expression (2), given by Keith and Weber (1964) and Babalola et al. (2023).

$$Z = 2.048(\delta^{13}C + 50) + 0.498(\delta^{18}O + 50) \quad (2)$$

If $Z > 120$, the limestones could be classified as marine; if $Z < 120$, they are materials generated in or affected by meteoric waters. Finally, if Z has values close to 120, the limestones should be classified as of undetermined origin.

The C-value plot, proposed by Zhao et al. (2007), was used to discriminate general climatic conditions throughout the deposition of the studied sediments. This parameter is calculated according to the next expression (3):

Ibex-Lavinianum zones (Nieto et al., 2023). In the studied interval of the CE section there is no record of the Gavilán Formation. Consequently, Nieto et al. (2023) state that the top of the Gavilán Formation and the bottom of the Zegrí Formation are heterochronous.

With respect to the calcareous nannofossil biostratigraphy of the studied area, there are data from the CE and PR sections already published. At CE section (Reolid et al., 2014), the base of the NJT5b Subzone is marked by the first occurrence of *Lotharingius sigillatus* around the Solare/Elisa ammonite Subzone boundary of the Emaciatum ammonite Zone, and the boundary between the NJT5/NJT6 zones is based upon the first occurrence of *Carinolithus superbus* around the Polymorphum/Serpentinum ammonite Zone boundary, considering the nannofossil biostratigraphic scheme proposed by Mattioli and Erba (1999) for the Tethyan Domain. According to the nannofossil zonation more recently proposed by Ferreira et al. (2019) for the Lusitanian Basin, the FO of *C. superbus* marks the beginning of the NJT6 Zone within the uppermost part of the Polymorphum Zone.

$$C-value = \Sigma(Fe + Mn + Cr + Ni + V + Co)/\Sigma(Ca + Mg + Sr + Ba + K + Na) \quad (3)$$

C-value comprised between 0 and 0.2, points to an arid climate. C-value between 0.2 and 0.4, refers to semi-arid climate. When this parameter is in a range 0.4–0.6, the climate is semiarid to semimoist. The values in the range between 0.6 and 0.8, shown a semimoist climate. Finally, if the C-value is higher than 0.8, recorded a moist climate.

4 Results

4.1 Biostratigraphy and chronostratigraphy

The biostratigraphy and chronostratigraphy related to the boundary between the Gavilán and Zegrí formations have just been studied in detail by Nieto et al. (2023). These authors identified up to five discontinuities of hiatus with variable amplitude between them and between different stratigraphic sections.

At the bottom of the PEL section, cherty limestones have been recognized, alternating with marls (Figs. 2 and 3) attributed to the upper part of the Gavilán Formation. No features have been observed at the top of these limestones that would indicate the existence of a stratigraphic discontinuity. In the PR section, some limestones with cherts have been identified and attributed to the upper part of the Gavilán Formation (Figs. 2, 3). In this case, based on regional data, the hiatus associated with the discontinuity between the two formations has been considered to span the

In the PR section (Nieto et al., 2023), based upon the more recent biostratigraphic scheme of Ferreira et al. (2019) for the Western Tethys, the NJT5b Subzone has been identified based upon the FO of *L. crucicentralis* within the upper Pliensbachian and NJT5c Subzone (lower part of the Polymorphum Zone) considering the FO of *Zeugrhabdothus erectus*, which enabled the approximation of the upper Pliensbachian/lower Toarcian boundary.

A total of 26 species belonging to 14 genera were identified in the 23 smear samples from PEL section (check Table 1 for further details). Most of the samples belonging to the Gavilán Formation are barren or show a poor preservation, including only extremely rare specimens of *Schizosphaerella punctulata* and *Calcivascularis jansae*. This last species also occurs in the lowermost samples of the Zegrí Formation until sample PEL-46m. Excluding three samples (PEL-42, 27 and 13; Table 1), a considerable increase in both abundance and diversity, as well as a much better preservation, can be noted from sample PEL-45 up-section. They yield up to 16 different species (samples PEL-17 and 15) and are dominated by relatively well-preserved specimens of *Schizosphaerella puntulata, Calcivascularis jansae, Mitrolithus lenticularis* and *Lotharingius hauffii*. Considering the biostratigraphic scheme proposed by Ferreira et al. (2019), a nannobiohorizon has been identified in the PEL section (Figs. 2, 3): the first occurrence of *Zeugrhabdothus erectus* in sample PEL-20 (Table 1). This bioevent marks the boundary between the NJT5b/NJT5c subzones and helps to approach the Pliensbachian/Toarcian boundary.

4.2 Facies analysis and ichnofacies

4.2.1 Facies and microfacies analysis

The PEL section begins in the cherty limestones of the top of the Gavilán Formation (first 5 m; Figs. 2, 4A). The microfacies are wackestone of radiolaria and sponge spicule (Fig. 5A) with *Thalassinoides* densely bioturbated by *Phycosiphon*. There are also very small (less than 0.15 mm in size) crinoidal fragments and other unidentifiable small bioclasts. The siliceous radiolarian tests have been replaced by microcrystalline calcite, obscuring their textural details. The siliceous megasclere spicules, mainly monaxon, have also been dissolved, and their moulds are filled with granular calcite cement. The rest of the section (NJT5 Zone), spans around 50 m and consists of marls and marly limestones of the Zegrí Formation (Figs. 2, 4B). The lower part of the Zegrí Formation, densely bioturbated (Fig. 4C), is dominated by limestone beds (first 13 m above the cherty limestones), followed by a thick interval of marls with carbonate

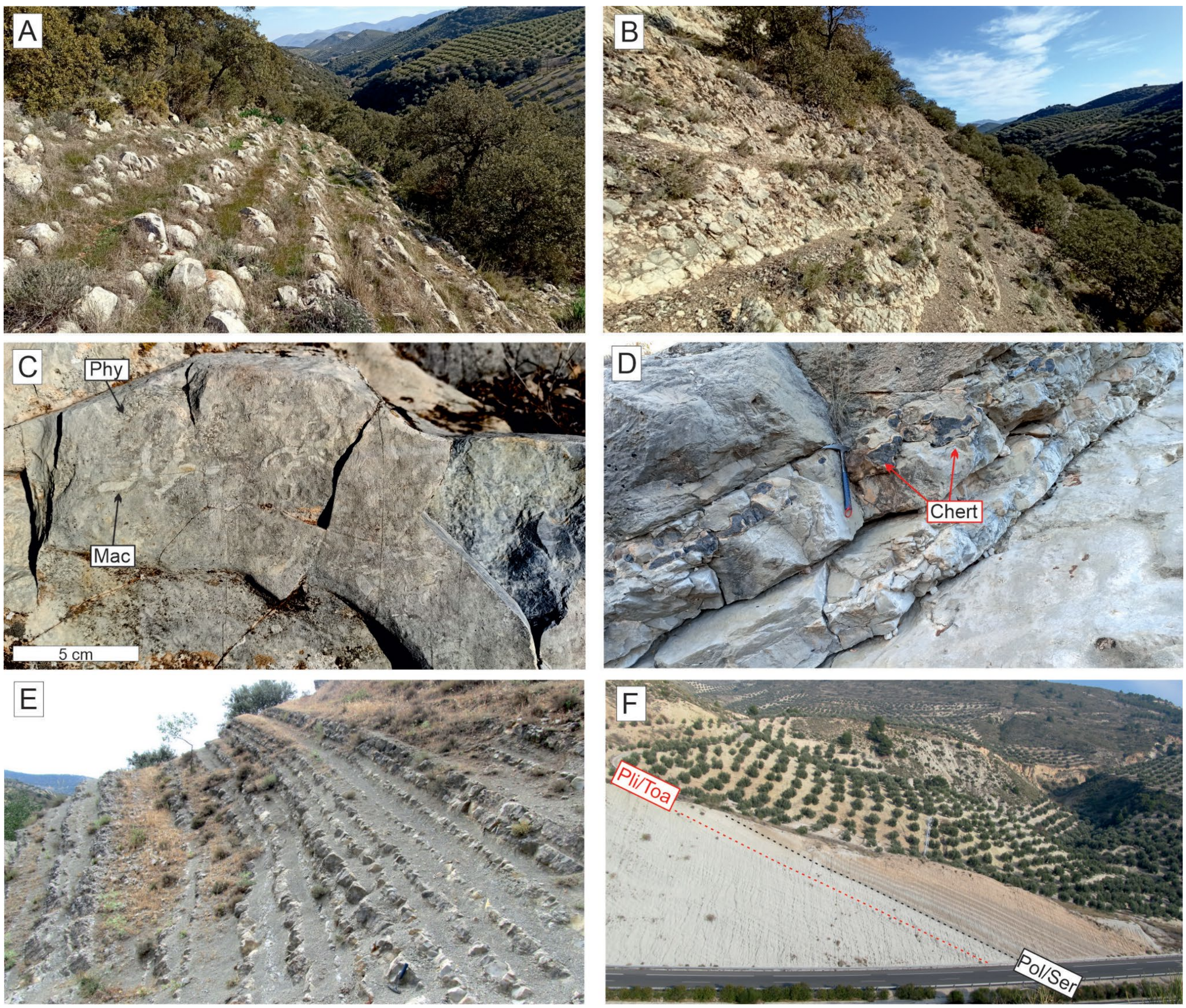

Fig. 4 Field view of the studied sections. **A** Top of the Gavilán Formation in the Sierra Pelada (PEL) section (Median Subbetic). **B** Lower part of the Zegrí Formation in the PEL section (Median Subbetic). **C** Detail of the stratigraphic surface of a bed located in the lowermost Zegrí Formation (upper Pliensbachian, PEL section) with abundant *Macaronichnus* (Mac) and *Thalassinoides*, the last one densely bioturbated by *Phycosiphon* (Phy). **D** Thick bedding in the top of the Gavilán Formation at the Puente Romano (PR) section (Median Subbetic), arrows point to black chert nodules. E. Marl-marly limestone alternation in the lower part of the Zegrí Formation at the PR section (Median Subbetic). **F** Marl and marly limestone rhythmite and overlying dark marls from the La Cerradura (CE) section (External Subbetic) with indications of the boundaries between Pliensbachian/Toarcian (Pli/Toa) and Polymorphum/Serpentinum zones (Pol/Ser) of the lower Pliensbachian

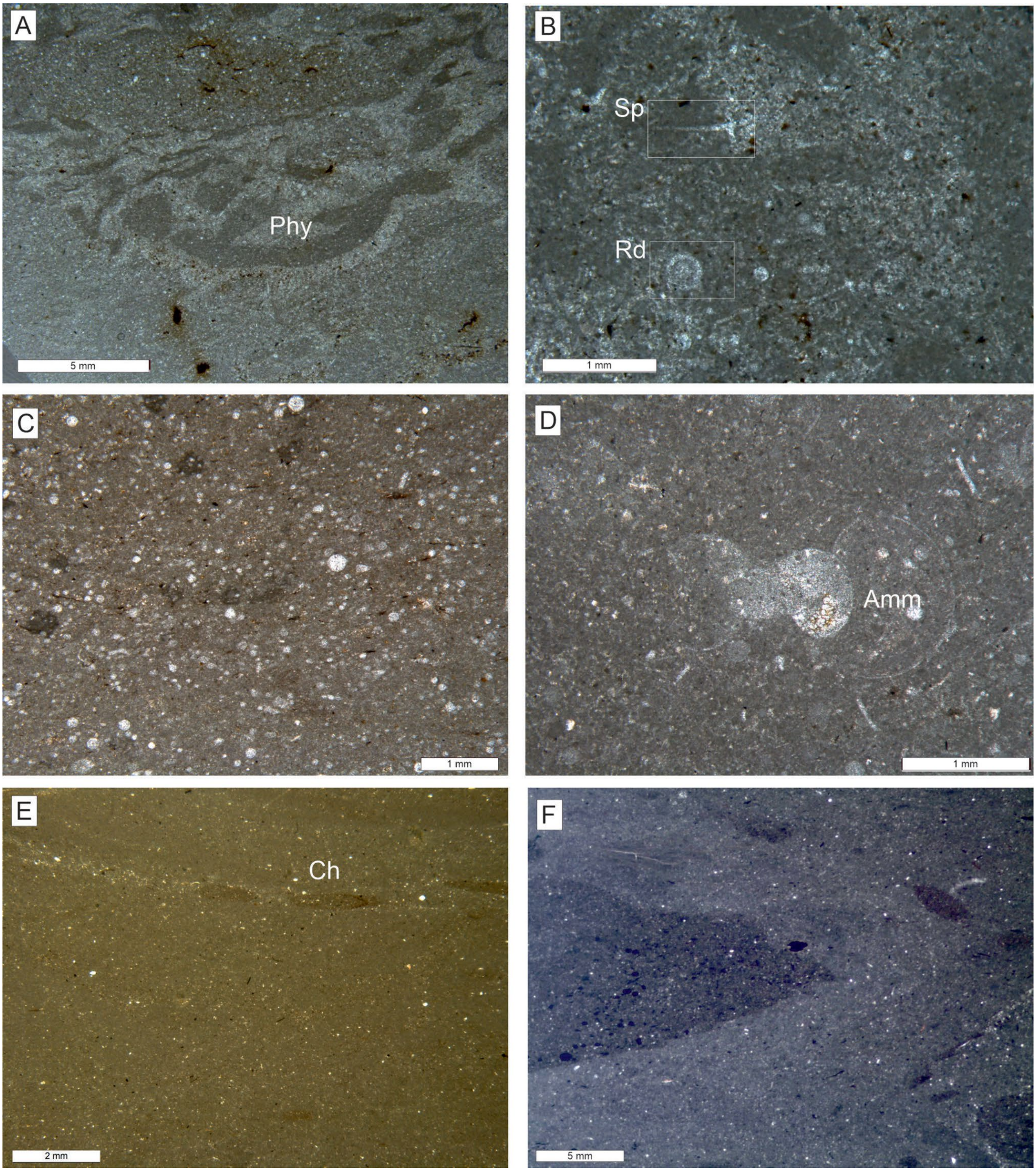

Fig. 5 Microfacies of the studied upper Pliensbachian-lower Toarcian sedimentary rocks of the Subbetic. **A** Microfacies of the top of Gavilán Formation with *Thalassinoides* densely bioturbated by *Phycosiphon* (Phy) (PEL section). **B** Detail of microfacies packstone of peloids, radiolarians (Rd) and sponge spicules (Sp) of the Zegrí Formation (PEL section). **C** Packstone of radiolarians from the Zegrí Formation (PR section). **D** Specimen of ammonite (Amm) of the packstone of radiolarians from the Zegrí Formation (PR section). **E** Mudstone to wackestone with trace fossils of *Chondrites* (Ch) from the Zegrí Formation (CE section). **F** Mudstone to wackestone with abundant coal grains (dark grains), specially concentrated in the dark areas corresponding to trace fossils, Zegrí Formation (CE section)

content increasing to the top of the sequences (around 25 m thick). The uppermost part of the studied section (within NJT5c Subzone, Polymorphum Zone, lower Toarcian) is composed of 12 m of marls and marly limestones alternation with progressive increase in carbonate content (Fig. 2). In PEL section, the microfacies differentiated for the Zegrí Formation (Fig. 5B) is a packstone of peloids, spicules and radiolaria with ostracods, calcispheres, benthic foraminifera (mainly *Lenticulina*) and some bioclasts. Small burrows are also observed in thin section, with common iron oxides or hydroxides. Locally, a mudstone with scarce radiolaria and bioclasts could be detected. Small burrows are also present. The phytodetritus is locally abundant in darker stratigraphic intervals.

In the PR section (Fig. 2) the studied interval corresponds to the Zegrí Formation and begins on the cherty limestones of the Gavilán Formation (Fig. 4D) (Nieto et al., 2023). The microfacies of the Gavilán Formation are peloidal and bioclastic wackestone-packstone (Fig. 5C, D). The peloids have an average size of 0.1 mm. The bioclasts are mainly crinoids, and secondarily sponge spicules, radiolarians, and thin-shelled bivalves ("filaments"). Subordinate components are represented by benthic foraminifera (*Lenticulina*), ostracods and calcispheres. The lower 7 m of the section (NJT5a Subzone) are made up of a limestone/marl alternation overlain by an alternation of dark marls/marly limestones of the upper Pliensbachian-lowermost Toarcian (Fig. 4E).

The CE section consists of a lower part constituted by marl and marly limestone alternation (Fig. 4F) (Emaciatum Zone, NJT5a and NJT5b subzones) and an upper part represented by a dark marls interval of the Serpentinum Zone (NJT6 Zone) (Fig. 2). The microfacies are mudstone-wackestone with trace fossils (Fig. 5E), in which abundant coal grains are concentrated (Fig. 5F). Unlike in the other sections of the Median Subbetic, in the CE section there are no radiolarians and sponge spicules.

4.2.2 Ichnofacies

In the PEL section (Fig. 6C, D), the ichnoassemblage recorded in the top of the Gavilan Formation is characterized by abundant horizontal to oblique sinuous burrows corresponding to *Macaronichnus* and secondarily *Thalassinoides*, *Planolites*, *Chondrites*, and *Zoophycos*. Other rare trace fossil is *Lamellaeichnus*. In the Zegrí Formation, the ichnoassemblage is similar with dominant *Macaronichnus* densely packed. *Phycosiphon* is very common burrowing within *Thalassinoides* sediment infilling. Secondary trace fossils are *Thalassinoides*, *Planolites*, *Zoophycos* and *Chondrites*, and less commonly *Lamellaeichnus* and *Palaeophycos*. *Macaronichnus* and *Phycosiphon* are infilled with clear sediment. In the case of *Macaronichnus* the mantle is comparatively darker than the surrounding sediment whereas the sediment infilling is clearer. The bioturbation index keeps very high in both formations in the PEL section ranging 3 to 5. The diversity is variable from 4 to 7 ichnogenera corresponding to the Cruziana ichnofacies. This diverse assemblage presents a good tiering with *Macaronichnus* and *Thalassinoides* dominating the upper tier, and *Zoophycos* and *Chondrites* dominating the lower tier.

The ichnoassemblage of the PR section (Fig. 6A, B) is similar to that described in the Zegrí Formation of the CE section by Reolid et al. (2014) and Simo and Reolid (2021). Commonly the trace fossils present a sediment infilling darker than the surrounding sediment. Some trace fossils present iron-rich sediment. Dominant trace fossils are *Planolites*, *Thalassinoides* and *Chondrites* (both large and small ones). Secondary trace fossils, but locally abundant, are *Lamellaeichnus*, *Teichichnus* and *Zoophycos*, and scarce *Palaeophycus* and *Taenidium*. The bioturbation index is commonly ranging from 2 to 3 and only decrease to 1 in the Pliensbachian/Toarcian boundary, where only scarce small *Chondrites* and *Planolites* are recorded. The number of ichnogenera in each level varies from 1 to 7 with lowest values located in the lower part of the NJT5a Subzone (upper Pliensbachian) and the top of the NJT5c Subzone (Polymorphum Zone, lower Toarcian). The lower part of the NJT5c Subzone records higher content of ferruginous trace fossils, principally *Chondrites* and *Planolites*. The trace fossils recorded in the PR section correspond to the Cruziana ichnofacies. The ichnoassemblage is relatively diverse and present a good tiering with *Planolites* and *Thalassinoides* dominating the upper tier, *Lamellaeichnus* and *Teichichnus* as main representants of a middle tier, and, finally, *Chondrites* and *Zoophycos* dominating the lower tier.

Finally, the ichnoassemblage of CE section (Fig. 6E) was studied by Reolid et al. (2014), Reolid and Reolid (2020) and Simo and Reolid (2021). This is mainly composed by *Planolites*, *Thalassinoides* and *Chondrites* (both small and large) and secondarily by *Lamellaeichnus*, *Taeinidum*, *Teichichnus* and *Trichichnus*. Other trace fossils such as *Zoophycos* and *Palaeophycus*, recorded in the PR section (Fig. 6A, B), or *Macaronichnus* and *Physosiphon* recorded in PEL section (Fig. 6C, D), are not present in CE section. In general, the bioturbation index and the diversity are similar to those of PR and lower than in PEL section, but decreasing in the NJT5b Subzone (Emaciatum Zone, upper Pliensbachian). The assemblage corresponds to the Cruziana ichnofacies. The ichnoassemblage is relatively diverse in the marl and marly limestone rhythmite, with *Planolites* and *Thalassinoides* dominating the upper tier, *Lamellaeichnus* and *Teichichnus* as main representants of a middle tier and, finally, small *Chondrites* dominating the lower tier. The bioturbation index is commonly ranging from 2 to 3, and decrease in the uppermost Pliensbachian and lower Toarcian where ranges from 1 to

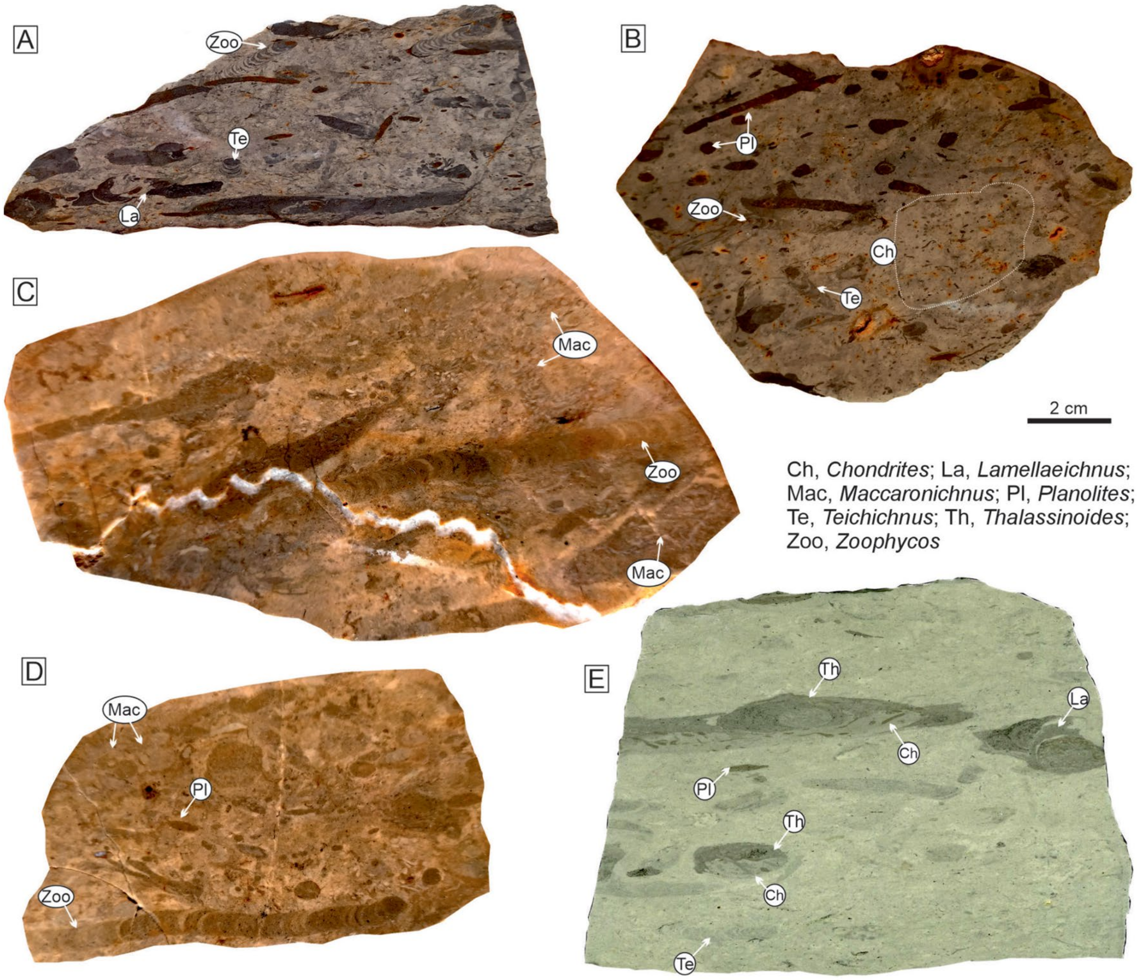

Fig. 6 Examples of ichnofossils in samples from the PR section (**A**, **B**), PEL section (**C**, **D**), and CE section (**E**)

2. The diversity is reduced in the beginning of the Toarcian, top of the marly limestone rhythmite (Polymorphum Zone, lower Toarcian) where *Chondrites* dominates. Only in the top of the Polymorphum Zone, large *Chondrites* turns very abundant and rich in organic matter (Reolid & Reolid, 2020). The first 40 cm of the dark marls of the Serpentinum Zone (coincident with the beginning of the negative CIE of the Jenkyns Event) are barren for infaunal benthic macroinvertebrates and trace fossils (Baeza-Carratalá et al., 2017; Reolid et al., 2014). The assemblage rapidly recovers initially with the record of *Chondrite*s, and subsequently with *Planolites* and *Trichichnus* (Simo & Reolid, 2021).

4.3 Geochemistry

4.3.1 δ^{13}C and δ^{18}O isotopes

The values of δ^{13}C (‰ VPDB) in PEL section fluctuate between – 0.41 ‰ and 1.22 ‰, (average 0.50 ‰, $\sigma = 0.39$). From the base of the stratigraphic section to meter 15, coinciding with the lowest rocks of the upper Pliensbachian in this section, the isotope ratio remains slightly above the average value (Fig. 2), although it shows some fluctuations in the first 5 m of the sequence and between meters 12.5 and 15 (Fig. 2). Between meters 15 and 27, coinciding with the lower part of the NJT5b Subzone (Emaciatum Zone, upper Pliensbachian), the marls are more abundant, in which there are many fluctuations, but always around the average. In the central part of the same subzone (between meters 27 and 30) a decrease of the isotope ratio values is observed, which varies between 0.50 and –0.41. From meter 30 onwards, there is an increase in the value of the isotopic ratio (from –0.41 to 0.53, obtained in meter 31). From this level to the top of the stratigraphic section, the $\delta^{13}C$ again shows several oscillations in its values, with a decreasing deviation respect to the average in the NJT5c Subzone (lower part of the Polymorphum Zone) (Fig. 2).

The $\delta^{18}O$ in the PEL section ranges between –4.43 and –2.25 ‰ (average – 3.52 ‰, $\sigma = 0.59$). As happened with the C isotope ratio, the $\delta^{18}O$ shows, in general, values slightly above the average between the base of the section and meter 15 (Fig. 2), coinciding with the levels dated as lower part of the upper Pliensbachian. Coinciding with the NJT5b Subzone (Emaciatum Zone, upper Pliensbachian), the values of this isotopic ratio are below the average, reaching the lowest values between meters 27 and 30, around the mid part of the NJT5b Subzone (Fig. 2). In the NJT5c Subzone, the $\delta^{18}O$ starts to increase its value until it is slightly above the average value.

In the PR section, the $\delta^{13}C$ values in the bulk sample change between 0.47 and 1.45 ‰ (Fig. 2) (average 1.11 ‰, $\sigma = 0.17$). In general, the values of this isotopic ratio show very little variations around the average value throughout the stratigraphic section, with no trend to be highlighted. Regards $\delta^{18}O$, the values range from –2.76 ‰ to –0.67 ‰ (average –2.17 ‰, $\sigma = 0.33$). Although the complete stratigraphic sequence shows numerous small-range fluctuations, all they are around the average, with no clear trends (Fig. 2).

In the CE section the values of $\delta^{13}C$ in bulk sample range between 0.41 and 1.93 ‰, (average 1.35, $\sigma = 0.32$). In the marl-marly limestone rhythmite (upper Pliensbachian to Polymorphum Zone; Fig. 2), they are at around 1.20 ‰. Above the top of the rhythmite (Fig. 2), a negative CIE is observed, changing the values of this isotope ratio from 1.20 to 0.41 ‰ (Fig. 2) corresponding to the lower part of the Serpentinum Zone (lower Toarcian). From meter 30, in the lower part of the Serpentinum Zone or lower part of the NJT6 Zone (Fig. 2), towards the top of the stratigraphic sequence, there is an increase in the value, from 0.41 to 2.47 ‰. The $\delta^{18}O$ shows a minimum value of –2.50 ‰ and the maximum value is –1.34 ‰ (average –1.96 ‰, $\sigma = 0.29$). This ratio decreases sharply in the Polymorphum Zone (lower Toarcian), where it reaches the minimum value, coinciding with the contact between the marl-marly limestone rhythmite and the dark marl interval. Here, an isotope excursion of –0.55 ‰ is recorded. In the base of the dark marls (top of the Polymorphum Zone; Fig. 2), a positive excursion (difference in isotope ratio of 1.00 ‰) is recorded, reaching a value of –1.50 ‰. After the first 2 m of the dark marls, the $\delta^{18}O$ ratio reaches values similar to those of the upper Pliensbachian.

4.3.2 Detrital and palaeoclimatic proxies

The Zr/Rb ratio in the PEL section (Fig. 7) shows high values at the base of the section that includes the top of the Gavilán Formation and the lower part of the Zegrí Formation (average 1.24, $\sigma = 0.13$; Fig. 7). The values decrease in the marl-dominated interval (NJT5b Subzone, Emaciatum Zone, upper Pliensbachian) and the upper part of the studied section (NJT5c Subzone, lower part of the Polymorphum Zone, lower Toarcian) (average 0.88, $\sigma = 0.08$). The Sr/Cu ratio shows a stratigraphic distribution with similar trends to Zr/Rb but the fluctuations are stronger (Fig. 7). Sr/Cu is higher in the lower part of the section (average 281.4, $\sigma = 122$) than in the upper part (average 118.6, $\sigma = 83$). Respect to the CIA and C-value present the lowest values in the lower part of the section (CIA average 0.04, C-value average 2.27) before the NJT5b Subzone of the marl-dominated interval of the Zegrí Formation (CIA average 0.13, C-value average 9.74; Fig. 7). The values of these parameters increase and present stronger fluctuations in the rest of the section and describe an opposite stratigraphic distribution respect to the Sr/Cu ratio.

In the PR section (Fig. 8), two stratigraphic intervals are differentiated, a lower interval that includes the first 7 m corresponding to NJT5a Subzone (Algovianum Zone, upper Pliensbachian), and the upper part formed by 18 m including the NJT5b (Emaciatum Zone, upper Pliensbachian) and NJT5c Subzones (lower part of Polymorphum Zone, lower Toarcian). The Zr/Rb ratio (Fig. 8) presents relatively low values in the lower stratigraphic interval (from 0 to 8 m, NJT5a Subzone; Fig. 8) with small fluctuations (average 1.44, $\sigma = 0.05$), and then is followed by a relative increase of Zr/Rb in the upper stratigraphic interval (average 1.52, $\sigma = 0.08$). The Zr/Rb values progressively decrease in the lower Toarcian (NJT5c Subzone; Fig. 7). The Sr/Cu ratio shows high values in the lower part of the studied section with low fluctuations (average 41.4, $\sigma = 7.7$), whereas the upper part of the section is characterized by relatively low values (average 27.4) with high fluctuations ($\sigma = 13.1$). CIA exhibits low values (average 10.1) and minor fluctuation ($\sigma = 2.4$) in the lower part of the section (Fig. 8), then a slightly increasing trend is recorded with high values in the upper stratigraphic interval (average 14.2) and important fluctuations ($\sigma = 5.1$). Finally, C-value presents a stratigraphic distribution similar to CIA in the PR section (Fig. 8). The lower stratigraphic interval presents low values (average 0.18, $\sigma = 0.02$), whereas the upper stratigraphic interval records high values with abrupt fluctuations (average 0.23, $\sigma = 0.05$).

The Zr/Rb ratio of the CE section (Fig. 9) shows low values (mostly < 0.75) in the rhythmite of the lower part of the section (from 0 to 26 m, Emaciatum Zone, upper

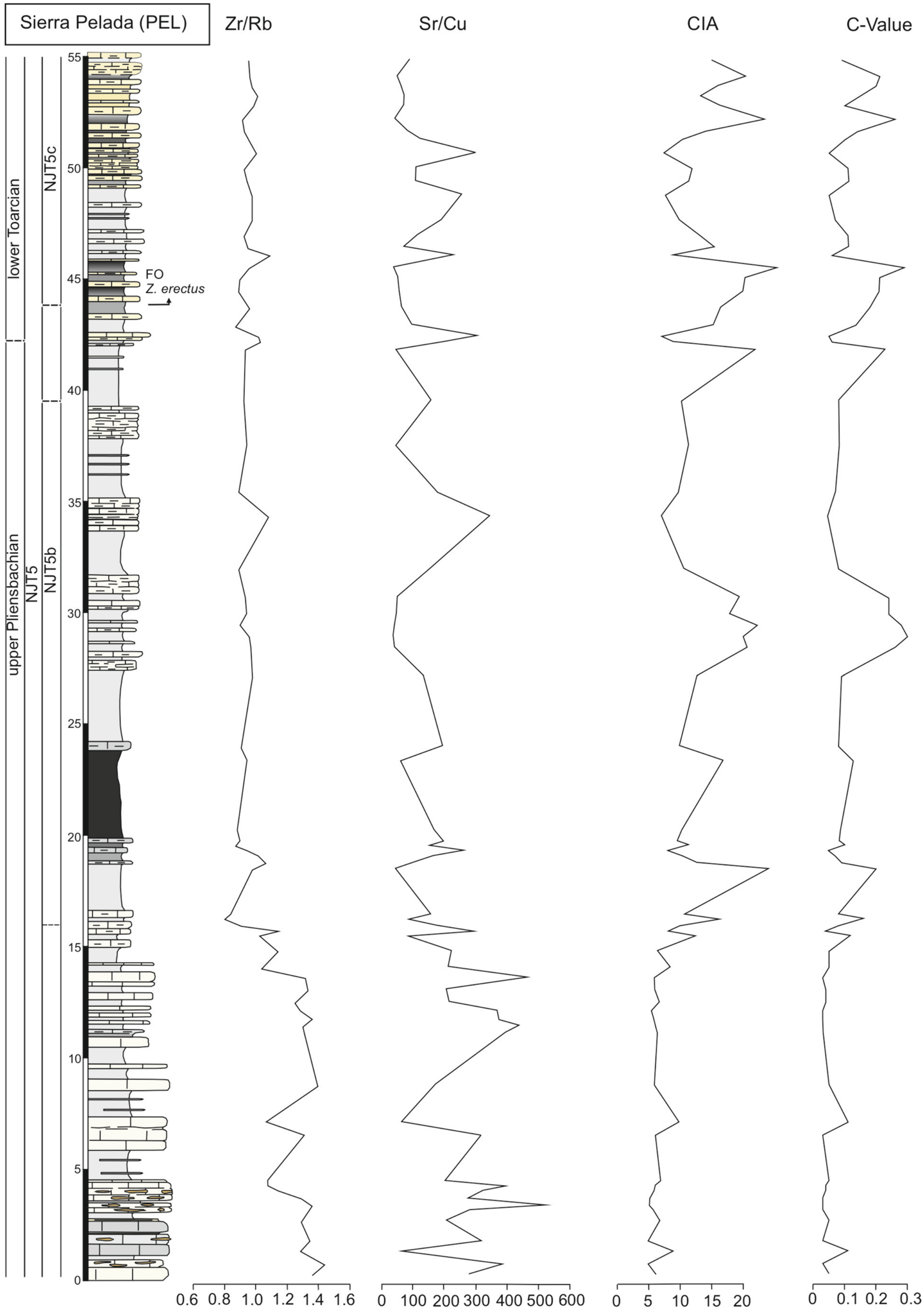

Fig. 7 Geochemical proxies of detritism from Sierra Pelada (PEL) section

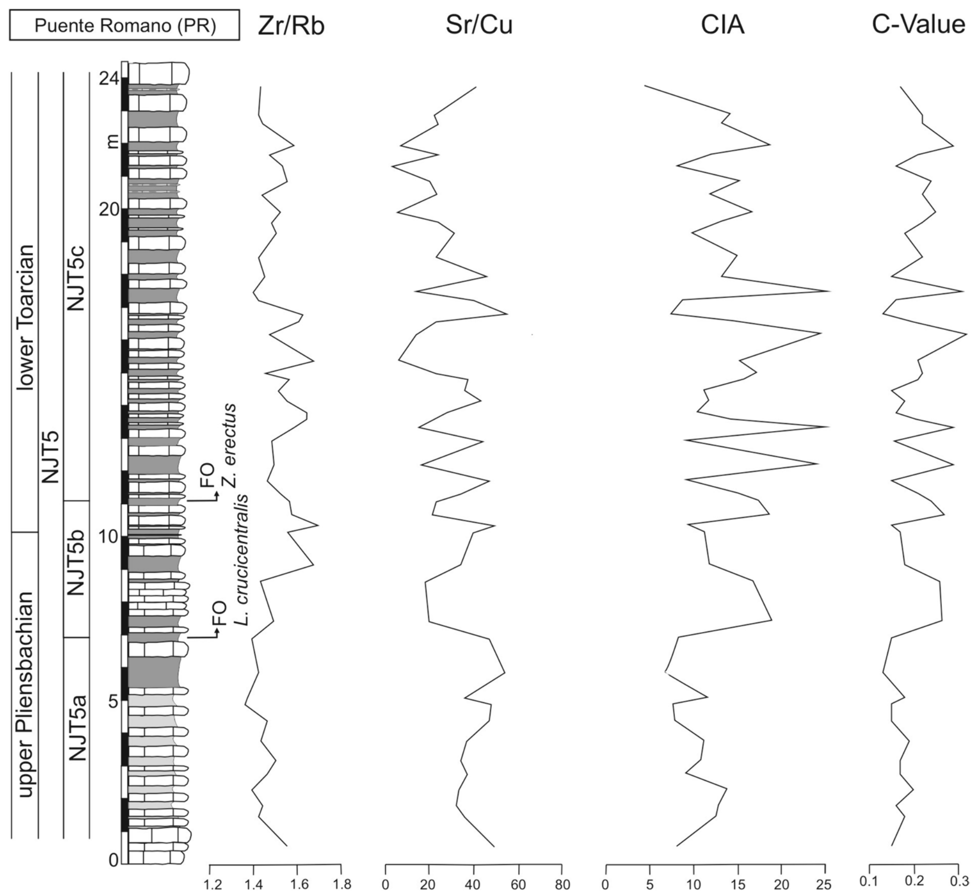

Fig. 8 Geochemical proxies of detritism from Puente Romano (PR) section

Pliensbachian; Fig. 9) with a Zr/Rb average value of 0.74 (σ = 0.03). The Zr/Rb values increase from the beginning of the dark marl (average 0.80, σ = 0.07) with important fluctuations and reaches the maximum during the negative Carbon Isotope Event (CIE). Respect to the Sr/Cu ratio, it shows relatively high values in the marl and marly limestone rhythmite (average 45.6, σ = 17.9) with the highest values in the lower part of the NJT5a Subzone, Emaciatum Zone (upper Pliensbachian; Fig. 9). The top of the rhythmite (Polymorphum Zone; lower Toarcian) presents a prominent increase of Sr/Cu; however, the overlying dark marls (NJT6 Zone, Serpentinum Zone) are characterized by a significant depletion (average 18.3, σ = 8.4). Finally, CIA also shows two different parts with relatively low values in the rhythmite (average 13.8, σ = 6.1) and higher values in the dark marls (average 29.3, σ = 8.1; Fig. 9). C–value shows a stratigraphic pattern similar to CIA (Fig. 9), with the lowest values corresponding to the rhythmite (average 0.13, σ = 0.04) and higher values in the dark marls (average 0.27, σ = 0.07). The highest values correspond to the beginning of the Serpentinum Zone, during the negative CIE followed by a light decrease.

4.4 Diagenetic signature

Correlation diagrams between the two isotope ratios, $\delta^{13}C$ and $\delta^{18}O$, were plotted for the studied stratigraphic sections (Fig. 10). For the PEL and PR sections, the correlation is positive, with a low coefficient of determination ($R^2 = 0.43$) in the PEL section, and a value of $R^2 = 0.54$ in the PR section. However, in the CE section, both ratios show a negative correlation with a value of coefficient of determination of $R^2 = 0.16$ (Fig. 10).

The Fig. 11 shows the correlation diagrams between $\delta^{13}C$ and Sr (ppm) and between $\delta^{18}O$ and the Fe/Ca and Sr/Ca ratios, according to the proposal of Babalola et al. (2023). These authors use the degree of correlation (shown by the value of the coefficient of determination between both values, R^2) as an indicator of the primary origin of the geochemical values.

In the PEL section, the correlation between $\delta^{13}C$ and Sr (ppm) is clearly positive but low ($R^2 = 0.25$; Fig. 11A). The correlation between $\delta^{18}O$ and the Fe/Ca ratio ($R^2 = 0.33$, Fig. 11B), is negative and low, while between $\delta^{18}O$ and Sr/Ca there is no correlation ($R^2 = 0.04$, Fig. 11C). In the PR section, $\delta^{13}C$ and Sr (ppm) show a low positive correlation

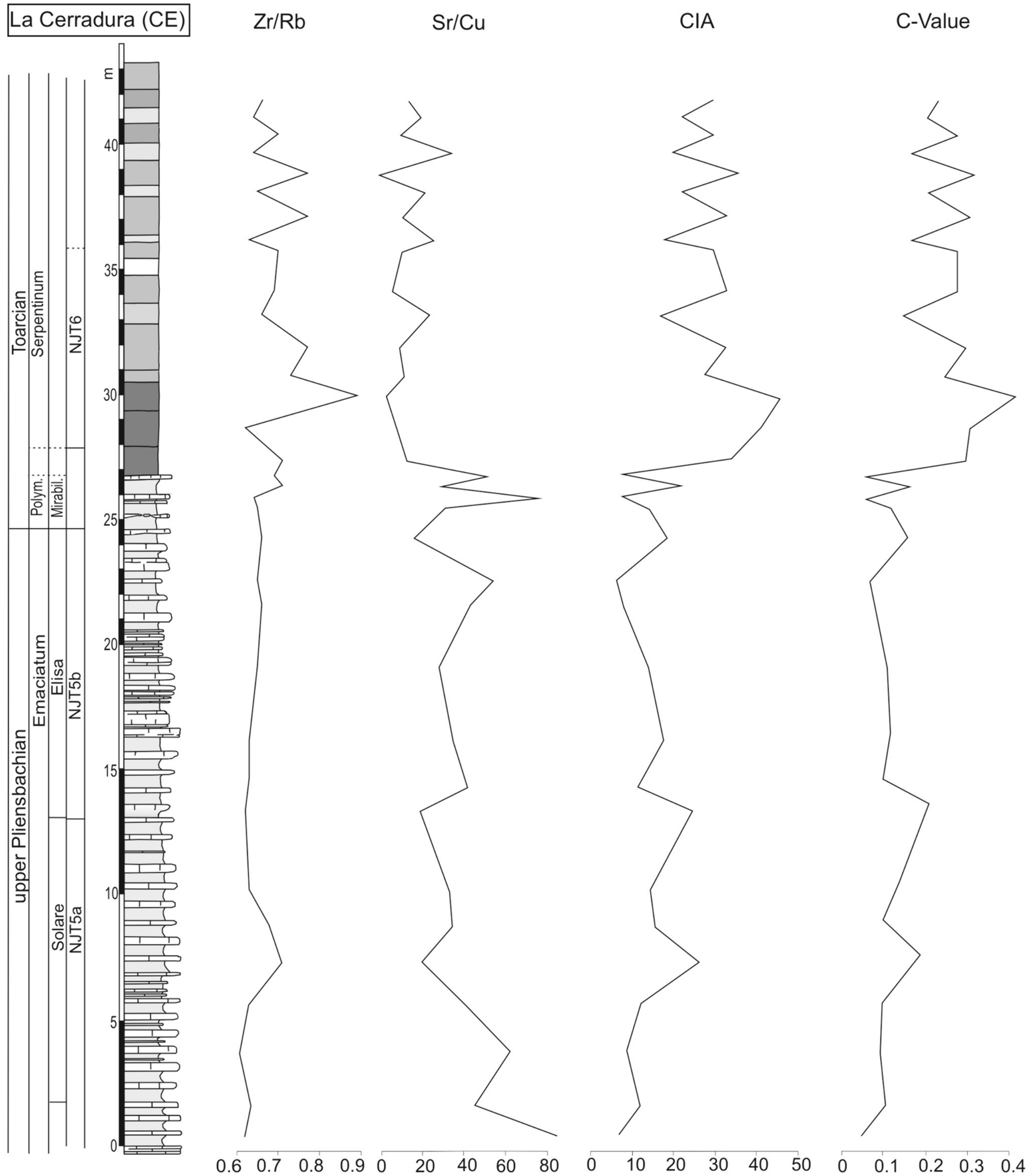

Fig. 9 Geochemical proxies of detritism from La Cerradura (CE) section

($R^2 = 0.26$, Fig. 11D). The correlation of $\delta^{18}O$ with Fe/Ca and Sr/Ca is low and negative ($R^2 = 0.36$ and 0.51 respectively, Figs. 11E, F). Finally, in CE section, the correlation between $\delta^{13}C$ and Sr (ppm) is slightly negative, with very low correlation ($R^2 = 0.002$, Fig. 11G). In the case of the correlations of $\delta^{18}O$ and the Fe/Ca ($R^2 = 0.53$) and Sr/Ca ($R^2 = 0.16$) ratios in CE section (Fig. 11H, I), are clearly negative.

In the studied sections the Z values is always > 120 (PEL section ranges between 124.31 and 128.67; PR section ranges between 127.00 and 129.94; CE section ranges between 127.48 and 130.33). Therefore, Z values confirm marine origin for the isotopic signal, and they have not undergone processes of meteoric diagenesis that have distorted their primary geochemical signature.

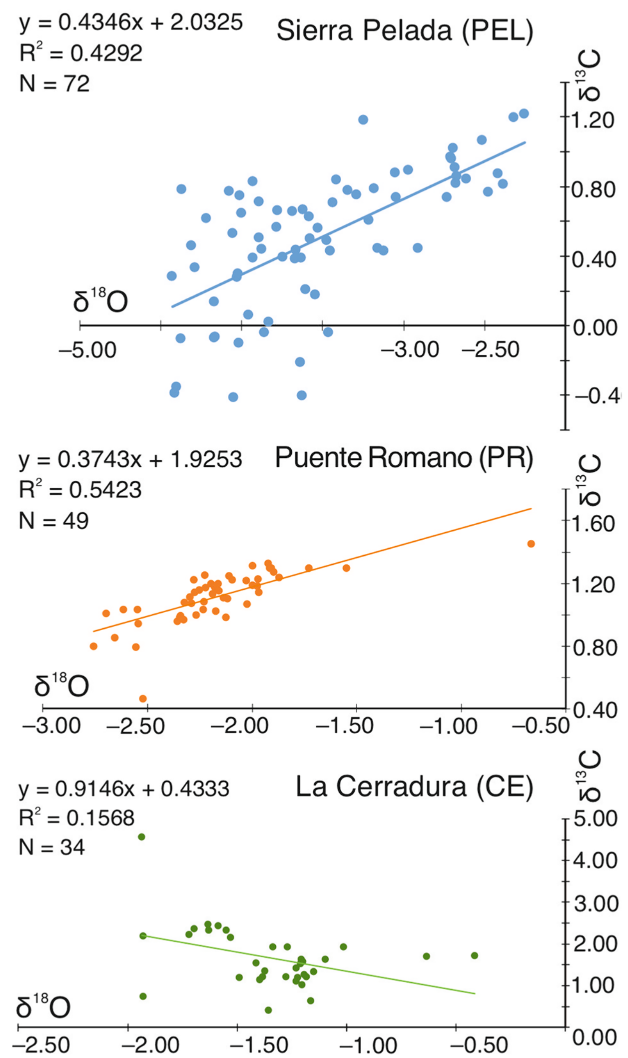

Fig. 10 Cross-plots of $\delta^{18}O$ versus $\delta^{13}C$ (V-PDB in ‰) for each stratigraphic sections studied with expression of correlation equation and the values of the coefficient of determination (R^2). In each plot, N means the number of samples analyzed

5 Discussion

5.1 Interpretation of facies and facies association

In the PEL and PR sections, materials attributed to the Gavilán Formation are recorded in the lower part of the successions. According to their microfacies and regional palaeogeographical context described before, the sediments were deposited in a distal carbonate platform. The presence of packstone with abundant peloids and crinoids supports the interpretation of a shallower depth and more energetic conditions for the deposits in the PR section, but the record of radiolarians confirms the hemipelagic influence. In the studied sections there are not sedimentary structures pointing to high energy conditions related to waves or tempestites, confirming a depositional setting above the storm wave base.

The beginning of the deposition of the rhythmite of the Zegrí Formation coincides with the start of the main phase of intracontinental breaking (rifting), developed from the early-late Pliensbachian (e.g. Nieto et al., 2023; Reolid et al., 2018). The bottom topography of the basin would be irregular with different semigrabens and changeful local subsidence and sedimentation rates (Nieto et al., 2004, 2023; Reolid et al., 2015; Vera, 2001), as is observed in other Tethyan Alpine domains (e.g. de Graciansky et al., 1998; Jenkyns, 2020; Marok & Reolid, 2012).

Respect to the Gavilán Formation, the Zegrí Formation represents a decrease in carbonate content mainly related to topographic changes at the sea bottom, with the development of troughs and swells (Nieto et al., 2023; Reolid et al., 2015, 2018; Vera, 2001), in addition to the transgressive regional and global context (e.g. de Graciansky et al., 1998; Hallam, 1987, 1997; Haq, 2018; Jenkyns, 1988; Korte & Hesselbo, 2011; Storm et al., 2020; Wignall et al., 2005). The alternation of grey marls and marly limestones of the Zegrí Formation represents a pelagic to hemipelagic environment, according to the record of ammonites, radiolarians, and siliceous sponge spicules. However, there is continental input evidenced by the terrigenous content of clay minerals, as reported for other areas of the Subbetic (Palomo, 1987; Rodríguez-Tovar & Reolid, 2013) and the described record of millimetric coal (wood) fragments and large coal fragments in the case of CE section (Reolid & Reolid, 2020; Reolid et al., 2019). There are not sedimentary structures pointing to high energy conditions.

The abundance of trace fossils in the studied sections confirms favourable conditions for infaunal organisms (oxygen and nutrient availability) as evidenced by previous papers in the Zegrí Formation for the upper Pliensbachian and Toarcian (Reolid et al., 2015; Rodríguez-Tovar & Reolid, 2013; Rodríguez-Tovar & Uchman, 2010; Simo & Reolid, 2021). The ichnoassemblages indicate a relatively soft ground with a good infaunal tiering. Only in the lowermost part of the dark marls of the Serpentinum Zone (NJT6 Zone) of the CE section, there is a sensible decrease of bioturbation that is locally absent during the beginning of the negative CIE (Reolid et al., 2014). Baeza-Carratalá et al. (2017) found specimens of a resilient assemblage of brachiopods in the dark marls, close to the base of the dark marls evidencing that some epifaunal forms survived.

The genetic interpretation of this rhythmic marl and marly limestone alternation is complex according to our recent data and needs to be studied to identify the Milanković cycles and to distinguish primary signatures of astronomically forced carbonate cycles (dilution, productivity or dissolution cycles) from the secondary effects of early diagenesis. Only in the case of the CE section there is a cyclostratigraphic

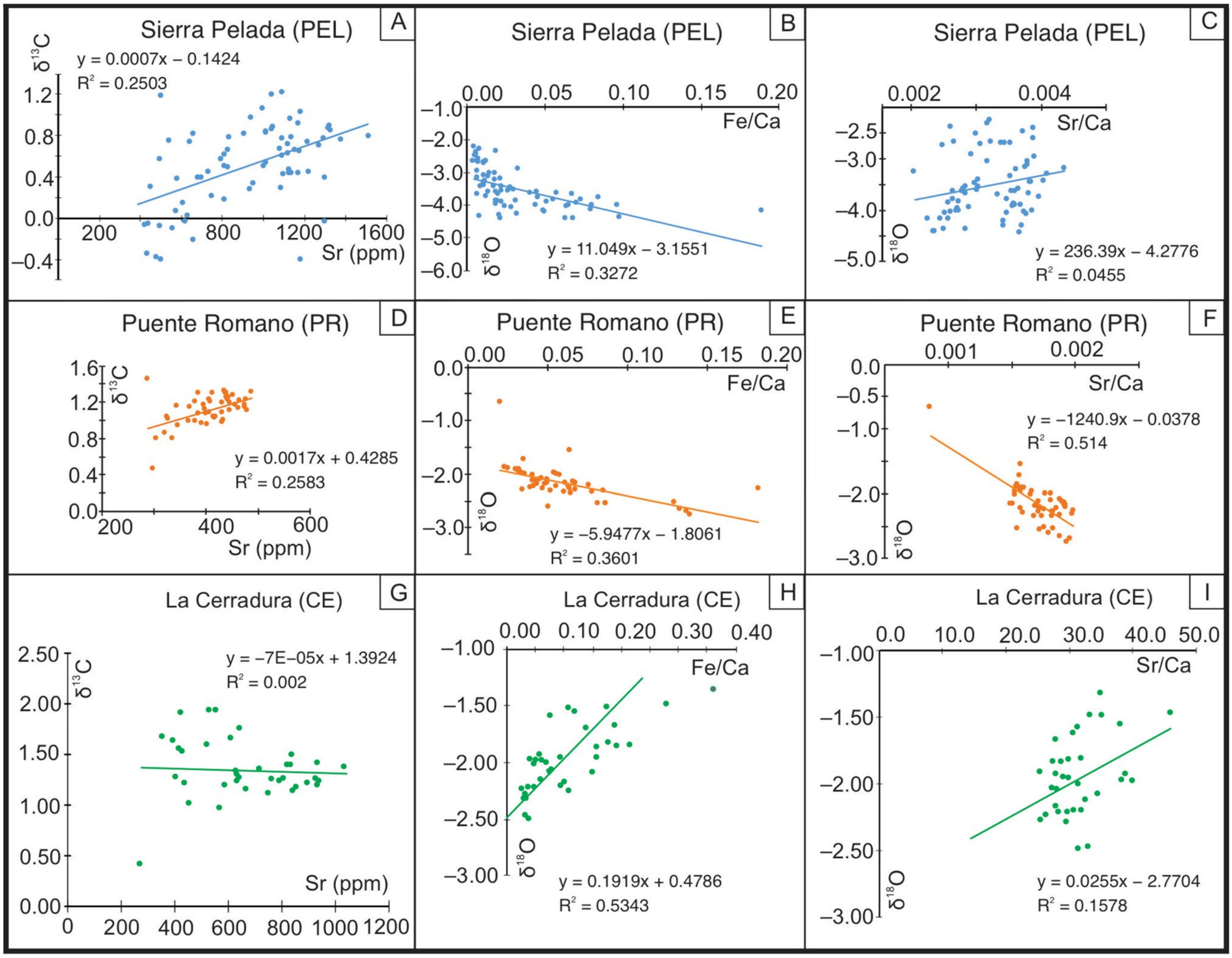

Fig. 11 Cross-plots of diagenetic elements, including Sr (in ppm) versus $\delta^{13}C$ and the Fe/Ca and Sr/Ca ratios versus $\delta^{18}O$ for each one of the stratigraphic sections studied. For each diagram the correlation equation and the coefficient of determination (R^2) is shown. The number of samples in each section is shown in the Fig. 10, PEL: N = 72; PR: N = 49; CE: N = 34

study that indicate orbital frequencies corresponding to long and short eccentricity mainly (Silva et al., 2021).

5.2 Diagenetic control in the primary geochemical proxies

A first approximation to the influence of diagenesis on the values of the different geochemical proxies considered can be made by comparing the $\delta^{13}C$ and $\delta^{18}O$ variation intervals with the ranges of variability of these same isotope ratios in other sections of the Western Tethyan Domain where materials of similar age are recorded (Fig. 12). From this comparison (Fig. 12) it is observed that the ranges of variation of both isotope ratios in the considered sections are shorter than those of other stratigraphic sections from different basins such as the Lusitanian Basin in Portugal (Duarte et al., 2014), the Iberian Basin in east Spain (Rosales et al., 2001), or the Atlasic Basin in Moroccan Atlas (Mercuzot et al., 2020). The Subbetic ranges are comprised within those of other basins. This is interpreted as meaning that diagenesis did not substantially modify the geochemical values and, therefore, they could be considered as primary.

Several authors have considered that the value of the correlation coefficient between $\delta^{13}C$ and $\delta^{18}O$ values in bulk sample can be a good signal of the intensity of diagenesis in carbonates (Babalola et al., 2023; Duchamp-Alphonse et al., 2007; Jenkyns & Clayton, 1986; Mercuzot et al., 2020). A low value of the coefficient of determination (R^2) could be interpreted as the record of a low-intensity diagenesis and, therefore, a primary origin could be attributed to the isotope values. In the sections studied in the Subbetic, R^2 is low (0.43 for PEL section, 0.54 for PR section, and 0.16 for CE section) (Fig. 10). However, Swart and Oehlert (2018) indicate that a low value of the coefficient of determination

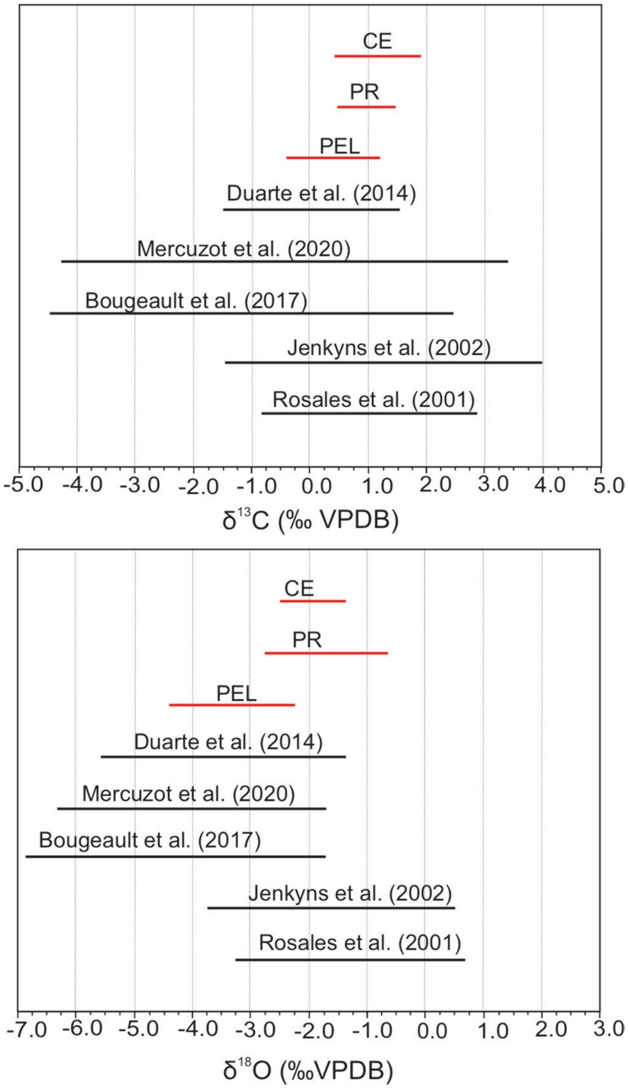

Fig. 12 Comparison of the range of variation of $\delta^{13}C$ (V-PDB in ‰) and $\delta^{18}O$ (V-PDB in ‰) in the three sections considered in this paper (CE: La Cerradura section; PR: Puente Romano section; and PEL: Sierra Pelada section) with the ranges of variation of these same isotope ratios in other Tethyan sections where coeval those studied in this research are recorded

or a lack of correlation between both isotope ratios should not necessarily indicate that the studied materials record the original isotope signal.

Babalola et al. (2023) make a detailed analysis of the influence of diagenesis in Middle Jurassic samples and propose that, in addition to the comparison of the fluctuation intervals of the isotope values, and the study of the coefficient of determination (R^2), the values of this coefficient obtained from the correlation of the isotope ratios with different elements (Fe, Ca, Mn, Sr) and some of their ratios (Fe/Ca, Sr/Ca, for example) could be considered. Figure 11 shows correlation diagrams of each of the isotope ratios with Sr, Fe/Ca and Sr/Ca for the studied sections. The coefficient of determination in all cases is very low for Sr and $\delta^{13}C$ ($R^2 < 0.26$), for Fe/Ca and $\delta^{18}O$ ($R^2 < 0.53$), and also for Sr/Ca and $\delta^{18}O$ ($R^2 < 0.51$). Considering the data as a whole, the values of the R^2 show values below 0.5, except in the CE section (Fe/Ca vs. $\delta^{18}O$) and in PR section (Sr/Ca vs. $\delta^{18}O$), with values slightly above 0.5. These values would indicate a weak diagenetic influence that would not substantially modify the primary geochemical signal. On the other hand, the values of the Z factor > 120 indicate that the studied materials are of marine origin and, therefore, with little or no influence of meteoric waters that have altered the primary diagenetic signal (Babalola et al., 2023). The scarce diagenetic effect on these sections is also confirmed by the microfacies where cements and radiolarians, sponge spicules and calcareous nannoplankton are generally preserved.

5.3 Carbon isotope stratigraphy

The $\delta^{13}C$ curves of the studied sections (Fig. 13) do not clearly show the excursions described for the Pliensbachian by Mercuzot et al. (2020). In the PEL section, between meters 42 and 46 (upper part of the NJT5b Subzone and lower part of the NJT5c Subzone) a negative excursion, correlatable with the Pliensbachian-Toarcian Boundary Event (PTBE) of Korte and Hesselbo (2011), Bodin et al. (2016), Fantasia et al. (2019), could be considered (Fig. 13). In the PR section, in a stratigraphic position equivalent to the one mentioned in the PEL section, the same event could also be identified. Finally, in the CE section, the PTBE is not observed, there is a clear negative CIE in the lower part of the Serpentinum Zone (NJT6 Zone, lower Toarcian) correlative with the Jenkyns Event as reported by Reolid et al. (2014) from $\delta^{13}C$ of bulk rock, and Ruebsam et al., (2020a, 2020b) and Kovács et al. (2024) from $\delta^{13}C$ of organic matter.

5.4 Palaeoclimatic changes

Important environmental changes can be identified according to the distribution of values of geochemical detrital proxies in PEL section. The lower part of the section, including the top of the Gavilán Formation and the lower part of the Zegrí Formation, records high values of Zr/Rb and Sr/Cu ratios that are interpreted as related to warm conditions. Sr/Cu is a weathering proxy that increases under warmer conditions (Bai et al., 2015; Cao et al., 2015; Moradi et al., 2016; Reolid et al., 2023). The Zr/Rb ratio is used as a proxy of the silt/clay ratio (Kylander et al., 2011) with Zr content related to eolian input (Pye, 1987; Hamroush and Stanley, 1990) and Rb related to fluvial transport to the basin (Chester et al., 1977; Reolid et al., 2012). That is, environmental conditions represented by the beginning of the Zegrí Formation in the Sierra Pelada section were arid and relatively warm. CIA

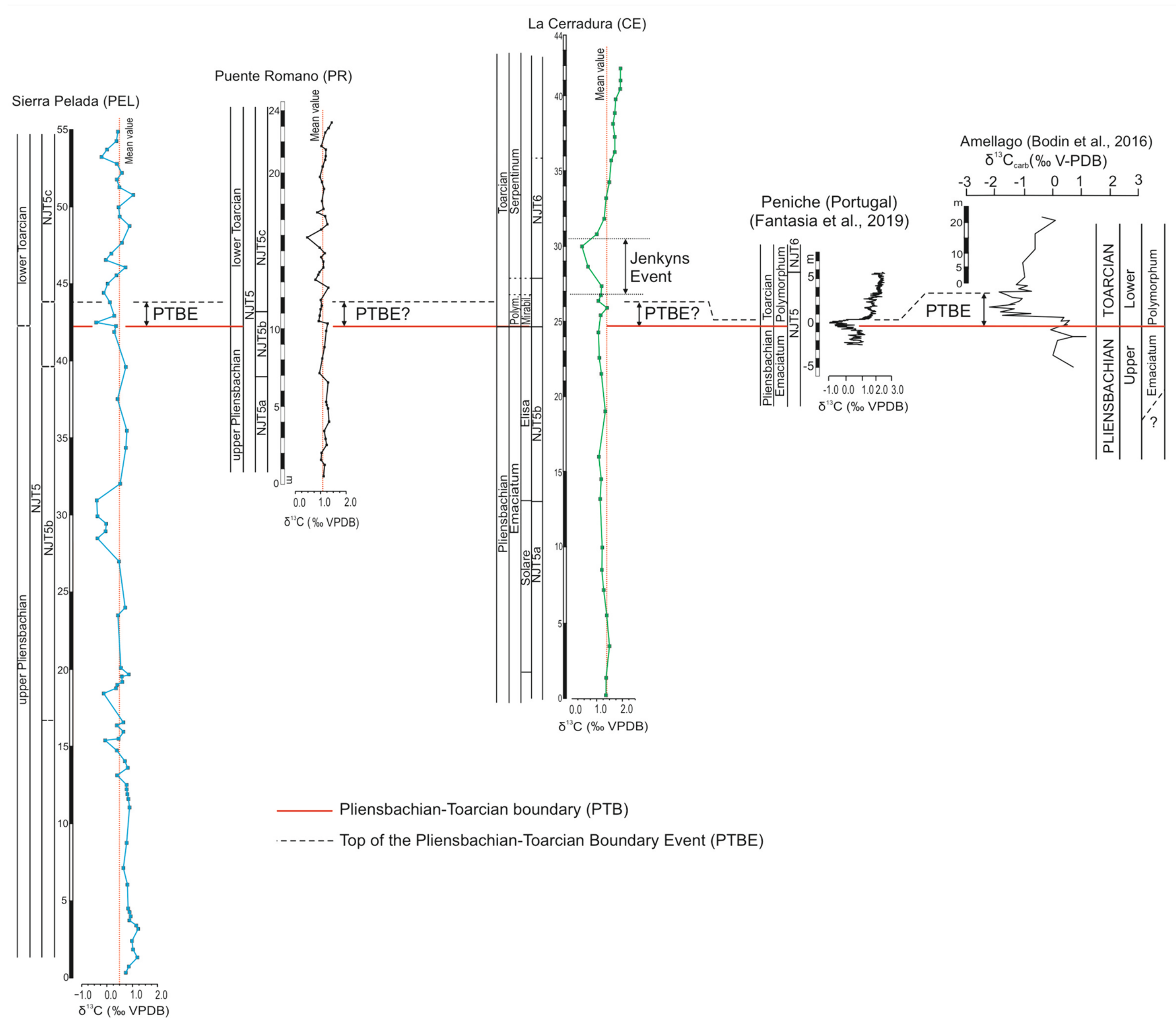

Fig. 13 Correlation of $\delta^{13}C$ curves of the sections considered in this paper with the curve of the Peniche section (Fantasia et al., 2019) and the Amellago section (Bodin et al., 2016). The possible location of the Pliensbachian-Toarcian Boundary Event (PTBE) in the sections studied in this paper is indicated from their position on the reference $\delta^{13}C$ curves

and C-value present the lowest values in this part of the section that confirm arid conditions.

In the marl dominated interval mainly corresponding to the NJT5b Subzone (Emaciatum Zone, upper Pliensbachian) and in the upper part of the studied section corresponding to the NJT5c Subzone (lower part of the Polymorphum Zone, lower Toarcian), the Zr/Rb ratio shows low values that indicate relatively humid conditions and enhanced fluvial input to the Median Subbetic. The Sr/Cu ratio shows a similar trend with stronger fluctuations that allow to interpret some warm episodes. The CIA and C-value have higher values in the NJT5b and NJT5c subzones than in the lower part of the section confirms an enhanced weathering and more humid conditions but probably abrupt fluctuations mainly in the early Toarcian as evidenced in the upper part of the section (NJT5c Subzone).

In the PR section two stratigraphic intervals were differentiated according to the geochemical detrital proxies. The lower interval of the Zegrí Formation corresponding to the NJT5a Subzone (Algovianum Zone, upper Pliensbachian) is characterized by relatively low Zr/Rb, CIA and C-values, as well as relatively high values of Sr/Cu. Relatively warm and arid conditions are evidenced from these data, however, relatively low values of Zr/Rb point to higher influence of fluvial input than eolian input for this part of the Median Subbetic.

From the NJT5b Subzone (Emaciatum Zone, upper Pliensbachian) there is an environmental change recorded by the increase of CIA and C-value that indicates enhanced weathering and moist conditions compared to the lower part of the section. A Zr/Rb increase occurs around the Pliensbachian/Toarcian boundary and lower part of the NJT5c Subzone (lower part of Polymorphum Zone, lower Toarcian) and indicate more arid conditions (more eolian input) which is opposite to the CIA and C-value interpretation. The Zr/Rb values progressively decrease across the lower Toarcian (NJT5c Subzone) pointing to higher incidence of fluvial inputs in the upper part of the section. The Sr/Cu shows strong fluctuations but a general decreasing trend in the lower Toarcian interpreted as relatively cold conditions (Cao et al., 2015; Moradi et al., 2016).

In CE section, the lower stratigraphic interval (marly limestone rhythmite of the upper Pliensbachian), is characterized by low Zr/Rb, CIA and C-value, that indicate dominance of fluvial detrital inputs and relatively low weathering. The Sr/Cu in this lower stratigraphic interval shows progressively decreasing values in the NJT5a Zone (Solare Subzone, Emaciatum Zone) that points to a cooling trend.

The top of the marly limestone rhythmite, corresponding to the Polymorphum Zone (lowermost Toarcian) evidences a perturbation herald of the Jenkyns Event with initial abrupt decrease of Sr/Cu in the Pliensbachian/Toarcian boundary correlated with a cooling episode, and a subsequent abrupt increase related to a warming.

The beginning of the dark marls of the Serpentinum Zone (NJT6 Zone, lower Toarcian), also characterized by a negative CIE (Kovács et al., 2024; Reolid et al., 2014; Ruebsam et al., 2020b), presents increasing values of Zr/Rb that indicate a stratigraphic shift in grain size for detritic input (Kylander et al., 2011) related to eolian sources congruent with more arid conditions interpreted for this palaeomargin by Rodrigues et al. (2019) from palynofacies. The Sr/Cu decrease points to a relative cooling climate that is contrary to the global warming interpreted after the study of $\delta^{18}O$ from belemnites (e.g. Danise et al., 2019; Fernández et al., 2020; Rosales et al., 2004) and brachiopods (e.g. Ferreira et al., 2019; Hesselbo et al., 2020b; Suan et al., 2010). The increasing CIA and C-value at the onset of the Jenkyns Event indicate enhanced continental weathering and sediment maturity under moist conditions. The highest values correspond to the beginning of the Serpentinum Zone, during the negative CIE followed by a light decrease.

5.5 Palaeogeographic considerations

In the previous section it has been shown that the geochemical signal of the detrital proxies analysed in each of the sections considered in this paper gives palaeoclimatic information that may be contradictory. For example, in the Algovianum Zone, the proxies indicating aeolian (Zr/Rb) or fluvial (Sr/Cu) influences show opposite trends in the PEL and PR sections. These disparities in geochemical signal indications could be interpreted considering the palaeogeographical position of the SIP in a zone of mixing of marine waters from the eastern Tethys and Panthalassa.

During the Davoei-Lavinianum Zones, the opening of the Hispanic Corridor (e.g. Price et al., 2016) occurred as a consequence of Central Atlantic rifting, which was also an important stage of volcanic activity of the Central Atlantic Magmatic Province and Karoo-Ferrar LIP (e.g., Krencker et al., 2022). The opening of this Corridor led to the establishment of a connection between Tethys and Panthalassa waters, the latter with a geochemistry that recorded the significant volcanic activity. In other words, a mixture of waters with a different geochemical imprint was produced (Dera et al., 2009a). In addition, the pattern of currents was modified, as the Viking Current, coming from Boreal domains to the South, disappeared and a current of waters, resulting from the mixing of the Panthalassa and Tethys waters, was established towards the North.

On the other hand, important changes occurred in the top of the Zegrí Formation in the sections considered. It is interesting to analyse the change in the materials attributed to the NJT5b Subzone of Ferreira et al. (2019), equivalent to the Emaciatum Zone (upper Pliensbachian) (Fig. 3), with a duration close to 720 ka, according to these authors (Fig. 3). These changes could be explained by (1) the development of sedimentary sub-basins (half grabens) in a rifting palaeotectonic context, with very different sedimentary input rates, (2) probable sediment by-pass situations due to the establishment of a new marine current system, and/or (3) differential subsidence controlled by rifting. Molina et al. (1999), Ruiz-Ortiz et al. (2004), Reolid et al. (2015) or Nieto et al. (2023), among others, indicate that, once the shallow-water carbonate platform of the lower Pliensbachian had disintegrated, a system of half-graben controlled by listric faults developed that could favor differences on subsidence, sedimentation rate, facies, and connection within different sub-basins in the SIP. The rate of sedimentation would be conditioned by sediment by-pass related to the action of currents and by a differential subsidence that would generate areas working as favorable depocenters.

In the CE section of the External Subbetic, the rocks attributed to the Elisa Subzone (that are close equivalent to the NJT5b Subzone of Ferreira et al., 2019) have a thickness of 11.2 m (Fig. 2). Considering this value and the duration of the subzone, a sedimentation rate of 0.018 mm/ka is estimated. In the PR section of the Median Subbetic, the thickness of the materials corresponding to this subzone is 4.24 m, which gives a sedimentation rate of 0.006 mm/ka. Finally, in the PEL section, also attributed to the Median Subbetic but located to the south, the rocks representing the NJT5b Subzone are 28.6 m thick, which gives a sedimentation rate of 0.040 mm/ka. From a palaeogeographical point of view, the External Subbetic is closer to the Iberian

Continent. This is congruent with the fact that palynomorphs of continental provenance have been recorded in the CE and Fuente Vidriera sections, both from the External Subbetic (Gambacorta et al., 2024; Rodrigues et al., 2019). On the other hand, the Median Subbetic would be arranged in palaeogeographical positions that would clearly belong to pelagic environments and where it must have been more difficult for continental inflows to reach.

In the case of the PEL section, where the sedimentation rate was higher (0.04 mm/ka), it was located in the most distal position and probably affected by Hispanic Corridor currents. The higher sedimentation rate and input of sediment from currents are the factors that explain this enhanced sedimentation rate. Moreover, the trace fossil assemblage dominated by *Macaronichnus*, not recorded in the southern studied sections, have been related to contourite depositional setting (Miguez-Salas et al., 2020). According to Rebesco et al. (2014) and Eberli and Betzler (2018), most of the described large contourite deposits are located in the western side of the largest oceanic basins, as well as around circumpolar basins. In the case of the SIP, it was located in the westernmost part of the Tethys Ocean, connecting with the Hispanic Corridor. This is congruent with the interpretation of the deposits of the Zegrí Formation in the PEL section as related to contour currents. *Macaronichnus* was related to sandy siliciclastic contourites (Miguez-Salas et al., 2022). This would be calcareous muddy contourites according to Rebesco et al. (2014) composing a carbonate drift as described by Reolid and Betzler (2018). The homogeneous and fine grain size as well as the dense bioturbation are not favorable for the identification of potential sedimentary structures related to currents such as lamination. Moreover, the dense accumulation of *Macaronichnus* indicates the abundance of nutrients in the environment (Miguez-Salas et al., 2020) and this trace fossil has been related to highly productive waters in connection with upwelling (Quiroz et al., 2019).

6 Conclusions

Three stratigraphic sections of the Betic External Zones were studied, two from the Median Subbetic, Sierra Pelada (PEL) and Puente Romano (PR), and one from the External Subbetic, La Cerradura (CE), where the Jenkyns Event was recorded by previous authors. In these sections, the upper Pliensbachian materials and the transition to the lower Toarcian were sampled bed by bed.

In the PEL and PR sections, the sedimentary successions were dated using calcareous nannoplankton. In the PEL section the NJT5b and NJT5c Subzones were recognized, whose boundary is marked by the FO of *Z. erectus*. In the PR section, the NJT5a, NJT5b, and NJT5c Subzones were recognised, whose boundaries coincide with FO of *L. crucicentralis* and FO of *Z. erectus*, respectively. In the CE section, both ammonite and calcareous nannoplankton biostratigraphies previously established by Reolid et al. (2014) were considered.

The dominant upper Pliensbachian facies in the three sections consist of a marly limestone-marl alternation. In both PEL and PR sections these same facies were dated as lower Toarcian, but in the CE section, this interval is represented by marls, in which Reolid et al. (2014) identified the Jenkyns Event. In the PEL section, *Macaronichnus* ichnofossil predominates. In the PR and CE sections, the ichnoassemblages are dominated by *Planolites*, *Thalassinoides* and *Chondrites*. The facies and ichnofacies observed were generated in hemipelagic marine environments influenced by continental sediments, as reflected in the clay contents studied by previous authors.

The analysis of the correlation between $\delta^{13}C$ and $\delta^{18}O$ and of these isotopic ratios with Sr and with Fe/Ca and Sr/Ca, respectively, show low or very low correlations, with values of the coefficient of determination (R^2) lower than 0.5; moreover, the Z factor presents values higher than 120 in the three sections, indicates a clear marine origin of the rocks studied. These parameters indicate that the geochemical signal has not been modified by diagenesis and can be considered to be of primary origin.

In the PEL and PR sections, the $\delta^{13}C$ and $\delta^{18}O$ ratios do not allow to clearly identify isotopic events during the late Pliensbachian, except for the transition to the early Toarcian, where the Pliensbachian-Toarcian Boundary Event (PTBE) could be recognized. In the CE section, where the Jenkyns Event was recorded, is not clear the recognition of the PTBE event.

The proxies used to study detritism (Zr/Rb, Sr/Cu, CIA and C-value) and to establish palaeoclimatic changes in the time interval studied show trends contrary to those detected in other sections from the Tethyan Domain and even among the sections studied here.

The geochemical signals, facies, microfacies and ichnofossil data were interpreted as the result of the opening of the Hispanic Corridor, associated with the Central Atlantic rifting stage, which favored the mixing of Panthalassa and Tethys seawaters, also establishing a system of currents towards Boreal domains. Extensional tectonics, which affected the SIP, favored the development of half grabens with important differential subsidence, especially during the NJT5b nannofossil Subzone (Emaciatum Zone, latest Pliensbachian). In addition, a possible by-pass effect of the established marine circulation system could transport sediments deposited in these half-grabens to other marine domains. This effect is clear in the PEL section (Median Subbetic), where the trace fossil assemblage, dominated by *Macaronichnus* and not recorded in the other two studied sections, were related to contourite depositional setting. Considering the palaeogeographic position of the SIP, in the westernmost part of the Tethys Ocean, and connected to the Hispanic Corridor, the existence of these contourite currents could have really occurred.

This paper highlights that the local oceanographic variables may play an important role at controlling the facies distribution and detrital input in highly complex and fragmented palaeomargins as this developed in South Iberia during the studied time interval.

Appendix A

Alphabetical listing including all the calcareous nannofossil species cited in the text with full author citations.

Calcivascularis jansae Wiegand 1984 (= *Mitrolithus jansae* sensu Bown and Young in Young et al., 1986).

Lotharingius crucicentralis (Medd, 1971) Grün and Zweili, 1980.

Lotharingius hauffii Grün and Zweili, 1974, emend. Goy, 1979.

Lotharingius sigillatus (Stradner 1961) Prins in Grün et al. 1974.

Mitrolithus lenticularis Bown 1987.

Schizosphaerella punctulata Deflandre and Dangeard, 1938.

Zeugrhabdotus erectus (Deflandre, 1954) Reinhardt, 1965.

Acknowledgements The authors wish to acknowledge Antonio Piedra-Martínez and Mª José Campos, Technicians of the Laboratory of Geology (University of Jaén). LMN, JMM, CA and MR thank to RNM-200 Research Group of Junta de Andalucía. AF thanks to the Spanish research group UCM-900431 and the help of Samuel Almeida-Martín with the preparation of the nannoplankton samples.

Funding Funding for open access publishing: Universidad de Jaén/CBUA. This research was funded by FEDER UJA 2020 PROJECT, grant number 1380715, Research Project PY20_00111 (Junta de Andalucía) and the UJA Project Acción 1b POAIUJA-2024. The authors are grateful to both the editors of the journal and the anonymous reviewers whose valuable comments substantially improved the manuscript.

Data availability The data will be available in the repository of the University of Jaén.

Declarations

Conflict of interest The authors declare that there is no conflict of interest.

References

Babalola, L. O., Alqubalee, A. M., Kaminski, M. A., & Abdullatif, O. M. (2023). Stable carbon and oxygen isotope records in a Middle Jurassic carbonate sequence: Implications for paleoenvironmental, and sea-level fluctuation, central Saudi Arabia. *International Journal of Earth Sciences, 112*, 585–613. https://doi.org/10.1007/s00531-022-02261-7

Baeza-Carratalá, J. F., Reolid, M., & García Joral, F. (2017). New deep-water brachiopod resilient assemblage from the South-Iberian Palaeomargin (Western Tethys) and its significance for the brachiopod adaptive strategies around the Early Toarcian Mass Extinction Event. *Bulletin of Geosciences, 92*, 233–256.

Bai, Y., Liu, Z., Sun, P., Liu, R., Hu, X., Zhao, H., & Xu, Y. (2015). Rare earth and major element geochemistry of Eocene fine-grained sediments in oil shale- and coal-bearing layers of the Meihe Basin, northeast China. *Journal of Asian Earth Sciences, 97*, 89–101.

Bassoullet, J.-P., Elmi, S., Poisson, A., Ricou, L.E., Cecca, F., Bellion, Y., Guiraud, R., & Baudin, F. (1993). Mid Toarcian (184 to 182 Ma). In J. Dercourt, L.E. Ricou, B. Vrielynck (Eds.): *Atlas Tethys Palaeoenvironmental Maps*, 63–80, Gauthier-Villars, Paris.

Bodin, S., Fantasia, A., Krencker, F. N., Nebsbjerg, B., Christiansen, L., & Andrieu, S. (2023). More gaps than record! A new look at the Pliensbachian/Toarcian boundary event guided by coupled chemo-stratigraphy. *Palaeogeography Palaeoclimatology Palaeoecology, 610*, 111344.

Bodin, S., Krencker, F. N., Kothe, T., Hoffmann, R., Mattioli, E., Heimhofer, U., & Kabiri, L. (2016). Perturbation of the carbon cycle during the late Pliensbachian—early Toarcian: New insight from high-resolution carbon isotope records in Morocco. *Journal of African Earth Sciences, 116*, 89–104.

Bougeault, C., Pellenard, P., Deconinck, J. F., Hesselbo, S. P., Dommergues, J. L., Bruneau, L., Cocquerez, T., Laffont, R., Huret, E., & Thibault, N. (2017). Climatic and palaeoceanographic changes during the Pliensbachian (Early Jurassic) inferred from clay mineralogy and stable isotope (C-O) geochemistry (NW Europe). *Global and Planetary Change, 149*, 139–152.

Bown, P. R., & Young, J. R. (1998). Techniques. In P. R. Brown (Ed.), *Calcareous Nannofossil Biostratigraphy* (pp. 16–28). Kluwer Academic.

Braga, J.C. (1983). *Ammonites del Domerense de la Zona Subbética (Cordilleras Béticas, Sur de España)*. PhD Thesis, Universidad de Granada, 410 pp.

Cao, H., Guo, W., Shan, X., Ma, L., & Sun, P. (2015). Paleolimnological environments and organic accumulation of the Nenjiang Formation in the southeastern Songliao Basin. *China, Oil Shale, 32*, 5–24.

Chester, R., Baxter, G. B., Behairy, A. K. A., Connor, K., Cross, D., Elderfield, H., & Padghamm, R. C. (1977). Soil-sized eolian dusts from the lower troposphere of the eastern Mediterranean Sea. *Marine Geology, 24*, 201–217.

Danise, S., Clémence, M. E., Price, G. D., Murphy, D. P., Gómez, J. J., & Twitchett, R. J. (2019). Stratigraphic and environmental control on marine benthic community change through the early Toarcian extinction event (Iberian Range, Spain). *Palaeogeography, Palaeoclimatology, Palaeoecology, 524*, 183–200.

Dera, G., Brigaud, B., Monna, F., Laffont, R., Pucêat, E., Deconinck, J. F., Pellenard, P., & Durlet, C. (2011). Climatic ups and downs in a disturbed Jurassic world. *Geology, 39*, 215–218.

Dera, G., Pellenard, P., Neige, P., Deconinck, J. F., Pucéat, E., & Dommergues, J. L. (2009b). Distribution of clay minerals in Early Jurassic Peritethyan seas: Palaeoclimatic significance inferred from multiproxy comparisons. *Palaeogeography Palaeoclimatology Palaeoecology, 271*, 39–51.

Dera, G., Pucéat, E., Pellenard, P., Neige, P., Delsate, D., Joachimski, M. M., Reisberg, L., & Martinez, M. (2009a). Water mass exchange and variations in seawater temperature in the NW Tethys during the Early Jurassic: Evidence from neodymium and oxygen isotopes of fish teeth and belemnites. *Earth and Planetary Science Letters, 286*, 198–207.

Duarte, L. V., Comas-Rengifo, M. J., Silva, R. L., Paredes, R., & Goy, A. (2014). Carbon isotope stratigraphy and ammonite biochronostratigraphy across the Sinemurian-Pliensbachian boundary in the western Iberian margin. *Bulletin of Geosciences, 89*, 719–736.

Duchamp-Alphonse, S., Gardin, S., Fiet, N., Bartolini, A., Blamart, D., & Pagel, M. (2007). Fertilization of the northwestern Tethys (Vocontian basin, SE France) during Valanginian carbon isotope perturbation: Evidence from calcareous nannofossils and trace element data. *Palaeogeography Palaeoclimatology Palaeoecology, 243*, 132–151.

Eberli, G. P., & Betzler, C. (2018). Characteristics of modern carbonate contourite drifts. *Sedimentology, 66*, 1163–1191.

Fantasia, A., Adatte, T., Spangenberg, J.E., Font, E., Duarte, L.V., & Föllmi, K.B. (2019). Global v. local processes during the Pliensbachian-Toarcian transition at the Peniche GSSP, Portugal: a multi-proxy record. *Earth-Science Reviews*, *198*, art. 102932.

Fernández, A., Korte, C., Ullmann, C. V., Looser, N., Wohlwend, S., & Bernasconi, S. M. (2020). Reconstructing the magnitude of Early Toarcian (Jurassic) warming using the reordered clumped isotope compositions of belemnites. *Geochimica Et Cosmochimica Acta, 293*, 308–327.

Ferreira, J., Mattioli, E., Sucherás-Marx, B., Giraud, F., Duarte, L. V., Pittet, B., Suan, G., Hassler, A., & Spangenberg, J. E. (2019). Western Tethys Early and Middle Jurassic calcareous nannofossil biostratigraphy. *Earth-Science Reviews, 197*, 102908.

Fleischmann, S., Picotti, V., Rugenstein, J.C.K., Cobianchi, M., & Bernasconi, S.M. (2022). Effects of the Pliensbachian-Toarcian Boundary Event on Carbonate Productivity of a Tethyan Platform and Slope. *Paleoceanography and Paleoclimatology, 37*, e2021PA004392. https://doi.org/10.1029/2021PA004392.

Fraguas, Á., Comas-Rengifo, M. J., Goy, A., & Gómez, J. J. (2018). Upper Sinemurian-Pliensbachian calcareous nannofossil biostratigraphy of the E Rodiles section (Asturias, N Spain): A reference section for the connection between the Boreal and Tethyan Realms. *Newsletters on Stratigraphy, 51*, 227–244. https://doi.org/10.1127/nos/2017/0401

Fraguas, Á., Comas-Rengifo, M. J., & Perilli, N. (2015). Calcareous nannofossil biostratigraphy of the Lower Jurassic in the Cantabrian Range (northern Spain). *Newsletters on Stratigraphy, 49*, 179–199. https://doi.org/10.1127/nos/2015/0059

Franceschi, M., Dal Corso, J., Posenato, R., Roghi, G., Masetti, D., & Jenkyns, H. C. (2014). Early Pliensbachian (Early Jurassic) C-isotope perturbation and the diffusion of the *Lithiotis* Fauna: Insights from the western Tethys. *Palaeogeography Palaeoclimatology Palaeoecology, 410*, 255–263.

Gambacorta, G., Burmsack, H.-J., Jenkyns, H. C., & Erba, E. (2024). The early Toarcian Oceanic Anoxic Event (Jenkyns Event) in the Alpine-Mediterranean Tethys, north African margin, and north European epicontinental seaway. *Earth-Science Reviews, 248*, 104636. https://doi.org/10.1016/j.earscirev.2023.104636

García-Hernández, M., López-Garrido, A. C., Rivas, P., Sanz de Galdeano, C., & Vera, J. A. (1980). Mesozoic palaeogeographic evolution of the External Zones of the Betic Cordillera. *Geologie En Mijnbouw, 52*, 155–168.

Gómez, J. J., Comas-Rengifo, M. J., & Goy, A. (2016). Palaeoclimatic oscillations in the Pliensbachian (Early Jurassic) of the Asturian Basin (Northern Spain). *Climate of the past, 12*, 1199–1214.

González-Donoso, J. M., Rivas, P., & Vera, J. A. (1971). La serie liásica de Sierra Pelada (Zona Subbética, N. de Granada). *Cuadernos Geología Ibérica, 2*, 205–226.

De Graciansky, E-C., Jacquin, T. & Hesselbo, S.P. (1998). The Ligurian cycle: an overview of Lower Jurassic 2nd-order transgressive/regressive facies cycles in western Europe. In R-C. De Graciansky, J. Hardenbol, T. Jacquin and ER. Vail (Eds.): *Mesozoic and Cenozoic Sequence Stratigraphy of European Basins*. Soc. Econ. Paleontol. Mineral. Spec. Publ., *60*, 467–479.

Hallam, A. (1987). Radiations and extinctions in relation to environmental change in the marine Lower Jurassic of northwest Europe. *Paleobiology, 13*, 152–168.

Hallam, A. (1997). Estimates of the amount and rate of sea-level change across the Rhaetian—Hettangian and Pliensbachian—Toarcian boundaries (latest Triassic to early Jurassic). *Journal of the Geological Society, 154*, 773–779. https://doi.org/10.1144/gsjgs.154.5.0773

Hamroush, H. A., & Staley, D. J. (1990). Paleoclimatic oscillations in East Africa interpreted by analysis of trace elements in Nile delta sediments. *Episodes, 13*, 264–269.

Haq, B. U. (2018). Jurassic Sea-Level Variations: A Reappraisal. *GSA Today (geological Society), 28*(1), 4–10. https://doi.org/10.1130/GSATG359A.1

Hesselbo, S.P., Ogg, J.G. & Ruhl, M. (2020a). Chapter 26. The Jurassic Period. F.M. Gradstein, J.G. Ogg, M.D. Schmitz & G.M. Ogg (Eds.), *Geologic Time Scale 2020,* volume 2 (pp. 955–1021). Elsevier. https://doi.org/10.1016/B978-0-12-824360-2.00026-7

Hesselbo, S. P., Korte, C., Ullmann, C. V., & Ebbesen, A. L. (2020b). Carbon and oxygen isotope records from the southern Eurasian Seaway following the Triassic-Jurassic boundary: Parallel long-term enhanced carbon burial and seawater warming. *Earth-Science Reviews, 203*, 103131.

Jenkyns, H. C. (1988). The Early Toarcian (Jurassic) oceanic anoxic event: Stratigraphic, sedimentary, and geochemical evidence. *American Journal of Science, 288*, 101–151.

Jenkyns, H. C. (2020). The demise and drowning of Early Jurassic (Sinemurian) carbonate platforms: Stratigraphic evidence from the Italian peninsula, Sicily and Spain. *Atti Dei Convegni Lincei, 335*, 55–82.

Jenkyns, H. C., & Clayton, C. J. (1986). Black shales and carbon isotopes in pelagic sediments from the Tethyan Lower Jurassic. *Sedimentology, 33*, 87–106.

Jenkyns, H. C., Jones, C. E., Gröcke, D. R., Hesselbo, S. P., & Parkinson, D. N. (2002). Chemostratigraphy of the Jurassic System: Applications, limitations and implications for palaeoceanography. *Journal of the Geological Society of London, 159*, 351–378.

Jiménez, A.P. (1986). *Estudio paleontológico de los ammonites del Toarciense inferior y medio de las Cordilleras Béticas (Dactylioceratidae e Hildoceratidae).* PhD Thesis, Universidad de Granada, 252 pp.

Keith, M. L., & Weber, J. N. (1964). Carbon and oxygen isotopic composition of selected limestones and fossils. *Geochimica Et Cosmochimica Acta, 28*, 1787–1816. https://doi.org/10.1016/0016-7037(64)90022-5

Korte, C., & Hesselbo, S.P. (2011). Shallow marine carbon and oxygen isotope and elemental records indicate icehouse-greenhouse cycles during the Early Jurassic. *Paleoceanography, 26,* PA4219.

Kovács, E. B., Ruhl, M., Silva, R. L., McElwain, J. C., Reolid, M., Korte, C., Ruebsam, W., & Hesselbo, S. P. (2024). Mercury sequestration pathways under varying depositional conditions during Early Jurassic (Pliensbachian and Toarcian) Karoo-Ferrar volcanism. *Palaeogeography, Palaeoclimatology, Palaeoecology, 637*, 111977.

Krencker, F. N., Fantasia, A., El Ouali, M., Kabiri, L., & Bodin, S. (2022). The effects of strong sediment-supply variability on the sequencestratigraphic architecture: Insights from early Toarcian carbonate factory collapses. *Marine and Petroleum Geology, 136*, 105469.

Krencker, F. N., Lindström, S., & Bodin, S. (2019). A major sea-level drop briefly precedes the Toarcian oceanic anoxic event: Implication for Early Jurassic climate and carbon cycle. *Nature, 9*, 12518.

Kylander, M. E., Ampel, L., Wohlfarth, B., & Veres, D. (2011). High-resolution X-ray fluorescence core scanning analysis of Les Echets (France) sedimentary sequence: New insights from chemical proxies. *Journal of Quaternary Research, 26*, 109–117.

Marok, A., & Reolid, M. (2012). Lower Jurassic sediments from the Rhar Roubane Mountains (Western Algeria): Stratigraphic precisions and synsedimentary block-faulting. *Journal of African Earth Sciences, 76*, 50–65.

Mattioli, E., & Erba, E. (1999). Synthesis of calcareous nannofossil events in the Tethyan Lower and Middle Jurassic. *Rivista Italiana Di Paleontologia e Stratigrafia, 105*, 343–376.

Mercuzot, M., Pellenard, P., Durlet, Ch., Bougeault, C., Meister, Ch., Dommergues, J.-L., Thibault, N., Baudin, F., Mathieu, O., Bruneau, L., Huret, E., & El Hmidi, Kh. (2020). Carbon-isotope events during the Pliensbachian (Lower Jurassic) on the African and European margins of the NW Tethyan Realm. *Newsletters on Stratigraphy, 53*(1), 41–69.

Miguez-Salas, O., Dorador, J., Rodríguez-Tovar, F. J., & Linares, F. (2022). X-ray microtomography to approach bioturbation's influence on minor-scale porosity distribution: A novel approach in contourite deposits. *Journal of Petroleum and Engineering, 208*, 109251.

Miguez-Salas, O., Rodríguez-Tovar, F. J., & de Weger, W. (2020). *Macaronichnus* and contourite depositional settings: Bottom currents and nutrients as coupling factors. *Palaeogeography, Palaeoclimatology, Palaeoecology, 545*, 109639.

Molina, J.M. (1987). *Análisis de facies del Mesozoico en el Subbético Externo (Provincia de Córdoba y Sur de Jaén)*. PhD Thesis, Universidad de Granada, 518 pp.

Molina, J. M., Ruiz-Ortiz, P. A., & Vera, J. A. (1999). A review of polyphase karstification in extensional tectonic regimes: Jurassic and Cretaceous examples. Betic Cordillera, southern Spain. *Sedimentary Geology, 129*, 71–84.

Moradi, V. A., Sari, A., & Akkaya, P. (2016). Geochemistry of the Miocene oil shale (Hançili Formation) in the Çankiri-Çorum Basin, Central Turkey: Implications for paleoclimate conditions, source-area weathering, provenance and tectonic setting. *Sedimentary Geology, 341*, 289–303.

Nesbitt, H. W., & Young, G. M. (1982). Early Proterozoic climates and plate motions inferred from major element chemistry of lutites. *Nature, 299*, 715–717.

Nesbitt, H. W., & Young, G. M. (1989). Formation and diagenesis of weathering profiles. *Journal Geology, 97*, 129–147.

Nieto, L. M., Molina, J. M., & Ruiz-Ortiz, P. A. (2004). La Formación Zegrí: Registro de los primeros estadios de una etapa sinrift en el Jurásico de las Zonas Externas Béticas. *Geotemas, 6*, 157–160.

Nieto, L. M., Molina, J. M., Ruiz-Ortiz, P. A., Fraguas, Á., & Reolid, M. (2023). Evolution from Carbonate Platform to Pelagic Environments in the South Iberian Paleomargin (Pliensbachian–Early Toarcian, Early Jurassic): Carbonate Features and Isotope Geochemistry. *Minerals, 13*(11), 1386.

Palomo, I. (1987). *Mineralogía y geoquímica de sedimentos pelágicos del Jurásico inferior de las Cordilleras Béticas (SE de España)*. PhD Thesis, Universidad de Granada, 345 pp.

Perilli, N., Fraguas, A., & Comas-Rengifo, M. J. (2010). Reproducibility and reliability of the Pliensbachian calcareous nannofossil biohorizons from the Basque-Cantabrian Basin (N Spain). *Geobios, 43*, 77–85.

Price, G. D., Baker, S. J., Van De Velde, J., & Clémence, M. E. (2016). High-resolution carbon cycle and seawater temperature evolution during the Early Jurassic (Sinemurian-Early Pliensbachian). *Geochemistry, Geophysics, Geosystems, 17*, 3917–3928.

Pye, K. (1987). *Aeolian Dust and Dust Deposits*. Academic Press, 334 pp.

Quiroz, L. I., Buatois, L. A., Seike, K., Mángano, M. G., Jaramillo, C., & Sellers, A. J. (2019). The search for an elusive worm in the tropics, the past as a key to the present, and reverse uniformitarianism. *Scientific Reports, 9*, 18402.

Rebesco, M., Hernández-Molina, F. J., Van Rooij, D., & Wahlin, A. (2014). Contourites and associated sediments controlled by deep-water circulation processes: State-ot-the-art and future considerations. *Marine Geology, 352*, 111–154.

Reolid, M., Molina, J.M., Nieto, L.M., & Rodríguez-Tovar, F.J. (2018). *The Toarcian Oceanic Anoxic Event in the South Iberian Palaeomargin*. Springer Briefs in Earth Science, 122 pp.

Reolid, J., & Betzler, C. (2018). The ichnology of carbonate drifts. *Sedimentology, 66*, 1427–1448.

Reolid, J., & Reolid, M. (2020). Geochemical compositional mapping of Lower Jurassic trace fossils: Palaeoenvironmental significance and methodological implications. *Palaeogeography, Palaeoclimatology, Palaeoecology, 538*, 109456. https://doi.org/10.1016/j.palaeo.2019.109456

Reolid, M., Abad, I., & Benito, M. I. (2019). Upper Pliensbachian-Lower Toarcian methane cold seeps interpreted from geochemical and mineralogical characteristics of celestine concretions (South Iberian palaeo-margin). *Palaeogeography, Palaeoclimatology, Palaeoecology, 530*, 15–31.

Reolid, M., Mattioli, E., Duarte, L. V., & Ruebsam, W. (2021). The Toarcian Oceanic Anoxic Event: Where do we stand? In M. Reolid, L. V. Duarte, E. Mattioli, & W. Ruebsam (Eds.), *Carbon Cycle and Ecosystem Response to the Jenkyns Event in the Early Toarcian (Jurassic)* (p. 514). Geological Society.

Reolid, M., Mattioli, E., Nieto, L. M., & Rodríguez-Tovar, F. J. (2014). The Early Toarcian Oceanic anoxic event in the External Subbetic (Southiberian Palaeomargin, Westernmost Tethys): Geochemistry, nannofossils and ichnology. *Palaeogeography, Palaeoclimatology, Palaeoecology, 411*, 79–94.

Reolid, M., Rivas, P., & Rodríguez-Tovar, F. J. (2015). Toarcian ammonitico rosso facies from the South Iberian Paleomargin (Betic Cordillera, southern Spain): Paleoenvironmental reconstruction. *Facies, 61*, 22. https://doi.org/10.1007/s10347-015-0447-3

Reolid, M., Rodríguez-Tovar, F. J., Marok, A., & Sebane, A. (2012). The Toarcian Oceanic Anoxic Event in the Western Saharan Atlas, Algeria (North African Paleomargin): Role of anoxia and productivity. *Geological Society of America Bulletin, 124*, 1646–1664.

Reolid, M., Soussi, M., Ruebsam, W., Taher, I. B. H., Mattioli, E., Saidi, M., & Schwark, L. (2023). Ecosystem recovery after the Early Jurassic T-OAE in the Châabet El Attaris section of the Tunisian Atlas. *Palaeogeography, Palaeoclimatology, Palaeoecology, 631*, 111832.

Rodrigues, B., Silva, R. L., Reolid, M., Mendonça Filho, J. G., & Duarte, L. V. (2019). Sedimentary organic matter and $\delta^{13}C_{Kerogen}$ variation on the southern Iberian palaeomargin (Betic Cordillera, SE Spain) during the latest Pliensbachian-Early Toarcian. *Palaeogeography Palaeoclimatology Palaeoecology, 534*, 109342.

Rodríguez-Tovar, F. J., & Reolid, M. (2013). Environmental conditions during the Toarcian Oceanic Anoxic Event (T-OAE) in the westernmost Tethys: Influence of the regional context on a global phenomenon. *Bulletin of Geosciences, 88*, 697–712.

Rodríguez-Tovar, F. J., & Uchman, A. (2010). Ichnofabric evidence for the lack of bottom anoxia during the Lower Toarcian Oceanic

Anoxic Event (T-OAE) in the Fuente de la Vidriera section, Betic Cordillera, Spain. *Palaios, 25*, 576–587. https://doi.org/10.2110/palo.2009.p09-153r

Rosales, I., Quesada, S., & Robles, S. (2001). Primary and diagenetic isotopic signal in fossils and hemipelagic carbonates: The Lower Jurassic of northern Spain. *Sedimentology, 48*, 1149–1169.

Rosales, I., Quesada, S., & Robles, S. (2004). Paleotemperature variations of Early Jurassic seawater recorded in geochemical trends of belemnites from the Basque-Cantabrian basin, northern Spain. *Palaeogeography, Palaeoclimatology, Palaeoecology, 203*, 253–275.

Ruebsam, W., Mayer, B., & Schwark, L. (2019). Cryosphere carbon dynamics control early Toarcian global warming and sea level evolution. *Global and Planetary Change, 172*, 440–453.

Ruebsam, W., Reolid, M., Sabatino, N., Masetti, D., & Schwark, L. (2020a). Molecular paleothermometry of the early Toarcian climate perturbation. *Global and Planetary Change, 195*, 103351. https://doi.org/10.1016/j.gloplacha.2020.103351

Ruebsam, W., Reolid, M., & Schwark, L. (2020b). $\delta^{13}C$ of terrestrial vegetation records Toarcian CO_2 and climate gradients. *Science Reports, 10*(1), 117.

Ruebsam, W., & Schwark, L. (2021). Impact of north-hemispherical cryosphere on early Toarcian climate and environmental perturbation. *Geological Society London, Special Publications, 514*, 359–385. https://doi.org/10.1144/SP514-2021-11

Ruiz-Ortiz, P.A., Castro, J.M., Arias, C., Vilas, L., Martín-Chivelet, J., de Gea, G.A., Molina, J.M., Nieto, L.M., Reolid, M., Aguado, R., et al. (2019). The South Iberian Continental Margin. In C. Quesada, & T. Oliveira (Eds.), *The Geology of Iberia: a geodynamic approach, regional geology reviews*. Springer, (pp 190–205)

Ruiz-Ortiz, P. A., Bosence, D. W. J., Rey, J., Nieto, L. M., Castro, J. M., & Molina, J. M. (2004). Tectonic control of facies architecture, sequence stratigraphy and drowning of a Liassic carbonate platform (Betic Cordillera, Southern Spain). *Basin Research, 16*, 235–257.

Schöllhorn, I., Adatte, T., Charbonier, G., Mattioli, E., Spangenberg, J. E., & Föllmi, K. B. (2020b). Pliensbachian environmental perturbations and their potential link with volcanic activity: Swiss and British geochemical records. *Sedimentary Geology, 406*, 105665.

Schöllhorn, I., Adatte, T., Van de Schootbrugge, B., Houben, A., Charbonier, G., Janssen, N., & Föllmi, K. B. (2020a). Climate and environmental response to the break-up of Pangea during Early Jurassic (Hettangian-Pliensbachian); the Dorset coast (UK) revisited. *Global and Planetary Change, 185*, 1030096.

Silva, R. L., Rühl, M., Barry, C., Reolid, M., & Ruebsam, W. (2021). Pacing of late Pliensbachian and early Toarcian carbon cycle perturbation and environmental change in the westernmost Tethys (La Cerradura section, Subbetic Zone of the Betic Cordillera, Spain). *Geological Society London Special Publications, 514*, 387–408.

Simo, V., & Reolid, M. (2021). Palaeogeographical homogeneity of trace-fossil assemblages in Lower Jurassic spotted marls and limestones: Comparison of the Western Carpathians and the Betic Cordillera. *Geological Society London, Special Publications, 514*, 185–211.

Storm, M. S., Hesselbo, S. P., Jenkyns, H. C., & Gorbanenko, O. (2020). Orbital pacing and secular evolution of the Early Jurassic carbon cycle. *PNAS, 117*(8), 3974–3982. https://doi.org/10.1073/pnas.1912094117

Suan, G., Mattioli, E., Pittet, B., Lécuyer, C., Suchéras-Marx, B., Duarte, L. V., Philippe, M., Reggiani, L., & Martineau, F. (2010). Secular environmental precursors to Early Toarcian (Jurassic) extreme climate changes. *Earth and Planetary Science Letters, 290*, 448–458.

Swart, P. K., & Oehlert, A. M. (2018). Revised interpretations of stable C and O patterns in carbonate rocks resulting from meteoric diagenesis. *Sedimentary Geology, 364*, 14–23.

Taylor, A. M., & Goldring, R. (1993). Description and analysis of bioturbation and ichnofabric. *Journal of the Geological Society, 150*, 141–148.

Vera, J.A. (2001). Evolution of the southern Iberian continental margin. In P.A. Ziegler, W. Cavazza, A.H.F. Robertson, & S. Crasquin-Soleau, (Eds.), *Peri-Tethys Memoir 6: Peri-Tethyan Rift/Wrench Basins and Passive Margins*, vol. 186. Memoires du Museum National d'Histoire Naturelle Paris, pp. 109–143.

Vera, J.A. (Ed.) (2004). *Geología de España*. SGE-IGME.

Wignall, P. B., Newton, R. J., & Little, C. T. S. (2005). The timing of paleoenvironmental change and cause-and-effect relationships during the Early Jurassic mass extinction in Europe. *American Journal of Sciences, 305*, 1014–1032.

Zhao, Z., Zhao, J., Wang, H., Liao, J., & Liu, C. (2007). Distribution characteristics and applications of trace elements in Junggar Basin. *Natural Gas Exploration and Development, 30*, 30–33.